이학박사 학위논문

Study of Hysteretic Behavior in a Parametrically Modulated Cold Atomic System

매개변수 변조된 저온 원자계에서의 이력 거동 현상에 대한 연구

2016년 8월

서울대학교 대학원

물리·천문학부

이 완 희

Study of Hysteretic Behavior in a Parametrically Modulated Cold Atomic System

媒介變數 變調**된** 低溫 原子界**에서의** 履歷 擧動 現狀**에 대한** 硏究

指導敎授 諸元鎬

이 論文**을** 理學博士學位論文**으로** 提出**함**

2016年 **5** 月

서울大學校 大學院

物理·天文學部

李 完 熙

李完熙**의** 理學博士 學位論文**을** 認准**함**

2016年 **6** 月

委 員 長	안 경 원	印
副委員長	제 원 호	印
委 員	정 현 석	印
委 員	신 용 일	印
委 員	노 흥 렬	印

Study of Hysteretic Behavior in a Parametrically Modulated Cold Atomic System

by

Wanhee Lee, B.S.

Dissertation

Presented to the Faculty of the Graduate School of

Seoul National University

in Partial Fulfillment

of the Requirements

for the Degree of

Doctor of Philosophy

Seoul National University

August 2016

Abstract

Study of Hysteretic Behavior in a Parametrically Modulated Cold Atomic System

Wanhee Lee
Department of Physics and Astronomy
The Graduate School
Seoul National University

We performed dynamic and nonequilibrium phenomena studies by using trapped rubidium atom 85 in a parametrically modulated magneto-optical trap which has characteristics of the non-linear harmonic oscillator. The dynamic bistable state of our system is obtained by modulating the intensity of the trapping laser for the magneto-optical trap at twice of trap frequency. The nonlinear dynamic system is realized by adjusting the phase of modulated intensity of trap lasers such as the parametric resonant oscillator and the Duffing oscillation in our system and various nonlinear phenomena have been studied with these nonlinear dynamic systems.

The spontaneous discrete time-translational symmetry breaking transition occurs from dynamic bistable states of the system when the total number of atoms exceeds a certain number of atoms which is called the critical number. This phenomenon shows a very similar to the phase transition phenomena of mean-field model. Particularly, the hysteresis observed in the spontaneous discrete time-translational symmetry breaking transition when we change the

number of atoms with a constant rate. We predict that the hysteresis is generated by slowing down near the critical point. In addition, we study the universality class of the hysteresis with theoretical approaches. And we predicted that the hysteresis by sweeping the number of atoms is an analogy with the thermal hysteresis in mean-field model.

We measured the relaxation time at some points in spontaneous discrete time-translational symmetry breaking transition with changing the total number of atoms. The experimental results of relaxation time are demonstrated that the critical slowing down phenomenon occurs in our system which has longer relaxation time when it approaches the critical point. Furthermore, it has been described theoretically the relaxation time at each point from the mean-field equation of motion of the order parameter. In order to determine the physical characteristics of the hysteresis, we obtain experimentally the scaling exponents of hysteresis loop area and hysteresis width. These results are shown that the hysteresis in our system is similar to the thermal hysteresis in mean-field theory. From the study of thermal hysteretic behaviors in the parametrically modulated cold atomic system, we expect that our system is a good model for understanding the thermal hysteresis in various fields such as molecular switching, temperature driven metal-insulator transition (MIT) and antifreeze proteins (AFPs).

Keywords : nonequilibrium, parametric resonance, discrete time-translational symmetry breaking, mean-field theory, thermal hysteresis,

critical slowing down, scaling behavior

Student number : 2009-20422

Contents

List of Figures

Chapter 1

Introduction

The atomic physics has evolved with the advent of quantum mechanics, which started as an attempt to understand the internal structure of the atom, such as the atomic model of Bohr. To study the detailed internal structure of the atom as hyperfine structure, the interaction with light sources which have a coherence is analyzed and it was needed atoms which move slowly for precise measurements. The atomic physics made a great development with the laser cooling methods [1]. The technique of confining atoms move slowly by laser cooling with the magnetic field is succeeded. Steven Chu, Claude Cohen-Tannoudji and William D. Phillips won the Nobel prize for the technique to cool and trap atoms in 1997 [1, 2]. Magneto-Optical Trap method has been used in a variety of atomic physics. The ultra-cold atoms near the absolute zero temperature were made to overcome the limitations of the cooling method using a laser as evaporative cooling. And the theoretically predicted Bose-Einstein Condensate (BEC) was

realized in 1995 [8,9]. The realization of BEC led to the development of research for quantum gas such as degenerate Fermi gas [12, 13]. In recent years, various studies such as precision measurement with atomic interferometry and quantum information using ion trap have been progressed [10, 22].

Although the MOT system in atomic physics has obvious limitations, it is still important as studying the nonlinear and nonequilibrium dynamics in a many-body system. Since the MOT is the system which has cooperative effects between atoms due to the interaction with the light and precise and easy controllability of parameter of the system. We studied the nonequilibrium dynamics by the external field, the phase transition in nonequilibrium system and kinetic phase transition in our previous works [6, 7, 23].

It is important to understand non-equilibrium phenomena in a far from equilibrium system since the most of the natural phenomena occur in non-equilibrium conditions and it is still at early stages of its research. To understand non-equilibrium phenomena, various nonlinear oscillators, such as Duffing and parametric oscillators, have been studied in electric circuits, nano-mechanical beam oscillators, and trapped ion systems [1–3]. In addition, the modulated magneto-optical trap (MOT) system is also a good platform for studying the nonlinear oscillators [4,5]. In this system, the Duffing and parametric oscillators were implemented by modulating the intensity of lasers [6, 7].

Especially, the critical dynamics such as critical slowing down, one of nonequilibrium phenomena, have studied in an economy system, a biological system and solid state system [11–13,27]. And hysteresis, one of non-equilibrium

phenomena with varying temperature of system, is one of the most interesting topics that have been studied in various fields such as molecular switching using spin crossover [8–10], temperature driven metal-insulator transition (MIT) in solid state devices [5, 11], and antifreeze proteins (AFPs) in bionic system [6, 7].

In this thesis, we described the detailed experimental setup of parametrically modulated MOT system such as vacuum system, laser setup and its stabilization for realization of a parametric oscillator. In addition, the control systems of our experiments are described. (Chapter 2)

We briefly presented the parametrically modulated MOT system with theoretical description. Two phenomena that be caused the dynamics of our system, fluctuation-induced transition and light-induced inter-atomic interaction are described in this thesis. And we described the hysteresis as a response to the sweeping of the total number of atoms in the spontaneous symmetry breaking (SSB) transition. (Chapter 3)

The hysteresis as number sweeping in SSB transition is caused by the critical dynamics which is called the critical slowing down. In general, the time that a system takes recovery from a perturbed state, so-called relaxation time diverges near the critical point of the phase transition of the system. This phenomenon is called critical slowing down. We measure the relaxation time that takes to evolve to the stationary state after stopping the number sweeping and observe the slowing down phenomena in our system with the experimental results. (Chapter 4)

In addition, we described the theoretical approach to determine the

university class of the hysteresis by number sweeping through the mean-field model. It predicted that the hysteresis in our system is an analogy with the thermal hysteresis in the mean-field theory. We analyzed the scaling behavior of the hysteresis by measuring the scaling exponents of our system and it is the well-matched results with the theoretical expectation. By define a new scaling exponent of the hysteresis and study its physical meaning, we described the characteristics of our system. (Chapter 5)

And other work, the experimental setup and results in the ^{87}Rb MOT system are described in the Chapter 6. and the detailed calculations or experimental methods is attached in the appendix.

Bibliography

[1] S. Chu, L. Hollberg, J. E. Bjorkholm, Alex Cable, and A. Ashkin Phys. Rev. Lett. **55**, 48 (1985).

[2] P. D. Lett, R. N. Watts, C. I. Westbrook, W. D. Phillips, P. L. Gould, and H. J. Metcalf Phys. Rev. Lett. **61**, 169 (1988).

[3] D. A. W. Barton, S. G. Burrow, and L. R. Clare, J. Vib. Acoust. **132**, 021009 (2010).

[4] S. Zaitsev, O. Shtempluck, E. Buks, and O. Gottlieb, Nonlinear Dyn. **67**, 859–883 (2012).

[5] N. Akerman, S. Kotler, Y. Glickman, Y. Dallal, A. Keselman, and R. Ozeri, Phys. Rev. A **82**, 061402(R) (2010).

[6] K. Kim, H-R. Noh, and W. Jhe, Opt. Commun. **236**, 349 (2004).

[7] K. Kim, M-S. Heo, K-H. Kim, H-J. Ha, K. Jang, H-R. Noh, and W. Jhe, Phys. Rev. A **72**, 053402 (2005).

[8] K. Kim, M.S. Heo, K.H. Lee, K. Jang, H. R. Noh, D. Kim, and W. Jhe, Phys. Rev. Lett. **96**, 150601 (2006).

[9] G. Moon, Y. Kim, M-S. Heo, D. Ahn, J. Park, S. Shin, H-R. Noh, and W. Jhe, New J. Phys. **15**, 103030 (2013).

[10] R. G. Miller, S. Narayanaswamy, J. L. Tallon, and S. Brooker, New J. Chem. **38**, 1932 (2014).

[11] R. Kulamczewski, J. Olguin, J. A. Kitchen, H. L. C. Feltham, G. N. L. Jameson, J. L. Tallon, and S. Brooker, J. Am. Chem. Soc. **136**, 878 (2014).

[12] M. Shigeno, Y. Kushida, and M. Tamaguchi, Chem. Commun. **52**, 4955 (2016).

[13] S. Singh, M. R. Fitzsimmons, T. Lookman, J. D. Thompson, H. Jeen, A. Biswas, M. A. Roldan, and M. Varela, Phys. Rev. Lett. **108**, 077207 (2012).

[14] R. Xie, C. T. Bui, B. Varghese, Q. Zhang, C. H. Sow, B. Li, and T. L. Thong, Adv. Funct. Mater. **21**, 1602 (2011).

[15] Ö. Can and N. B. Holland, Biochemistry **52**, 8745 (2013).

[16] C. P. Garnham, R. L. Cambell, and P. L. Davies, PNAS **108**, 7363 (2011).

[17] M.H. Anderson, J.R. Ensher, M.R. Matthews, C.E. Wieman, and E.A. Cornell, Science **269**, 198 (1995).

[18] K. B. Davis, M. -O. Mewes, M. R. Andrews, N. J. van Druten, D. S. Durfee, D. M. Kurn, and W. Ketterle, Phys. Rev. Lett. **75**, 3969 (1995).

[19] B. DeMarco, J. L. Bohn, J. P. Burke, Jr., M. Holland, and D. S. Jin, Phys. Rev. Lett. **82**, 4208 (1999).

[20] F. Schreck, L. Khaykovich, K. L. Corwin, G. Ferrari, T. Bourdel, J. Cubizolles, and C. Salomon, Phys. Rev. Lett. **87**, 080403 (2001).

[21] G. Rosi, F. Sorrentino, L. Cacciapuoti, M. Prevedelli and G. M. Tino, Nature **510**, 518–521 (2014)

[22] L-M. Duan,and C. Monroe, Rev. Mod. Phys. **82**, 1209 (2010).

[23] M. S. Heo, Y. Kim, K. Kim, G. Moon, J. Lee, H=R. Noh, M. I. Dykman and W. Jhe, Phys. Rev. E. **82**, 031134 (2010).

[24] V. Guttal, S. Raghavendra, N. Geol and Q. Hoarau, Plos One 0144198 (2016).

[25] I. A. van de Leemput *et al.*, PNAS **111**, 87 (2014).

[26] R. A. Chisholm, E. Filotas, J. Theor. Biol. **257**, 142 (2009).

[27] D. Niermann, C.P. Grams, P. Becker, L. Bohatý, H. Schenck, and J. Hemberger, Phys. Rev. Lett. **114**, 037204 (2015).

Chapter 2

Experimental System

2.1 Introduction

The experimental setup of our system is basis on a conventional six-beam magnetic optical trap(MOT) of ^{85}Rb which has three orthogonal pairs of count-propagating beam and the intensities of laser on each axis are controlled by the acousto-optical modulator(AOM). A brief overview diagram for our system is shown in Figure 2.1 For achieving the parametric resonance in MOT, the intensity of trap laser on axis of anti-Helmholtz coil (z-axis of the system) is modulated as twice of trap frequency (about 150Hz). Also, the trap laser intensity of z-axis is weaker than the one of other axes, then the movement of atoms is approximated in one-dimensional [1]. For adjusting the total number of atoms in the system, we change the intensity of repumping laser and it was controlled by neutral density (ND) filter. To observe the movement of atoms

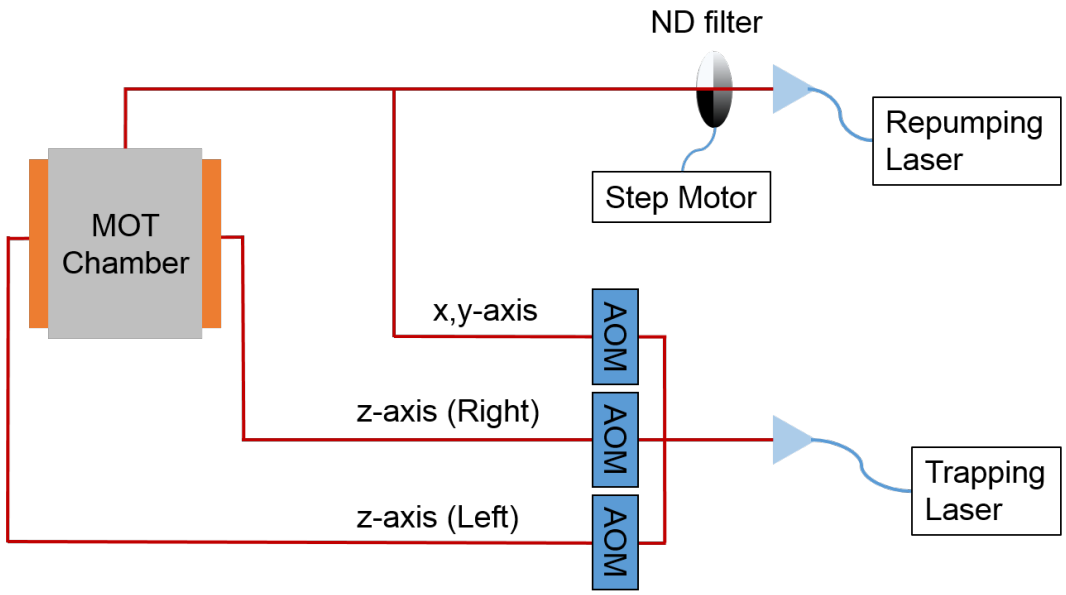

Figure 2.1: A schematic diagram of the experimental setup. The intensity of trapping laser is controlled independently by AOMs of each axis and the intensity of repumping laser is controlled by ND filter mounted on step motor.

in the parametrically modulated MOT and obtain a number of atom density distributions we used a charge-coupled device camera. More specific details of each part are explained in the next section.

2.2 Experimental Setup

2.2.1 Vacuum System

In order to trap the cold atoms by cooling effectively, the high vacuum system is essential. For this, we use stainless steel chamber which has 8 viewports with anti-reflection (AR) coating as shown in Fig. 2.2 (a). And we use the ion pump

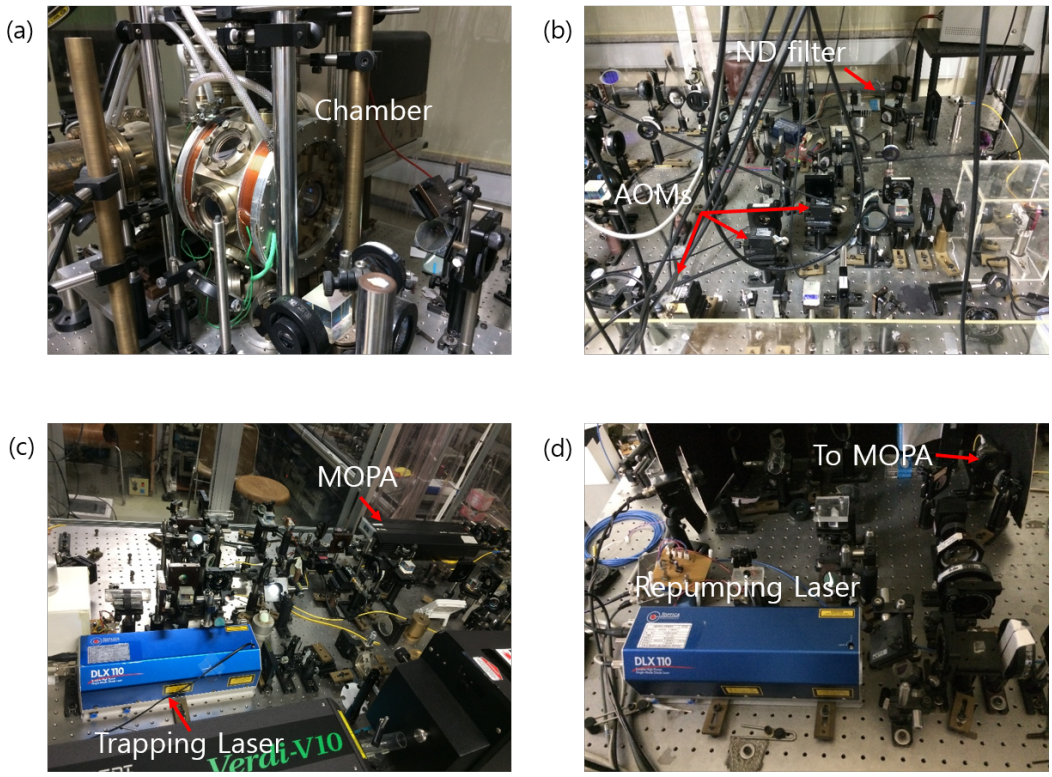

Figure 2.2: Photographs of Experimental Setup : (a) Chamber (b) Optics Setup (c) Trapping Laser and MOPA and (d) Repumping Laser.

(Duniway V220) of 220l/s to maintain the vacuum pressure as below 5×10^{-9} torr. The Rb getter is inside the chamber for supplying the rubidium atoms. In addition, the magnetic field gradient about 10G/cm was generated by the anti-Helmholtz coil which is attached outside of the chamber as shown Fig. 2.2 (a).

2.2.2 Laser Frequency Stabilization

We use two external cavity diode laser for trapping and repumping laser. Totica DLX110 laser (power 1W) for a trapping laser as shown in Fig. 2.2 (c) and another DLX110 laser is used but it is part of total power (about 100mW) for seeding laser as shown in Fig. 2.2 (d). To amplify the repumping laser power up to 300mW, we use the SDL-TC30 master oscillator power amplifier (MOPA) because it is more stable than using the DLX110 directly. In order to obtain the good Gaussian beam profile, all lasers are coupled with the single mode fibers and we use the three AOMs to manipulate the trapping laser intensity each axis independently. The laser frequency shift by the AOMs is from 70MHz to 110MHz. To realize the parametric oscillator in a cold atomic system. We need to stabilize the laser frequency below 1MHz precision and for this, we use the atomic hyperfine level as a reference for specific locked points of the laser frequency. We use the saturated absorption spectroscopy (SAS) and the modulation transfer spectroscopy (MTS) together to overcome the Doppler broadening of spectral line and resolve the hyperfine levels of rubidium atom [2–4]. We use the rubidium-85 D2 transition hyperfine structures as shown Fig. 2.3 and Fig. 2.4 for trapping lines (F=3 $\rightarrow$ F=2,3,4 transitions) and repumping lines (F=2 $\rightarrow$ F=1,2,3 transitions). The frequency of repumping laser is locked by top-of-fringe locking method at exact F=2 $\rightarrow$ F=3 transition line with the spectrum line of SAS. But the frequency of trapping laser is locked by the side-of-fringe locking method at the red-detuned F=3 $\rightarrow$ F=4 transition line with the spec-

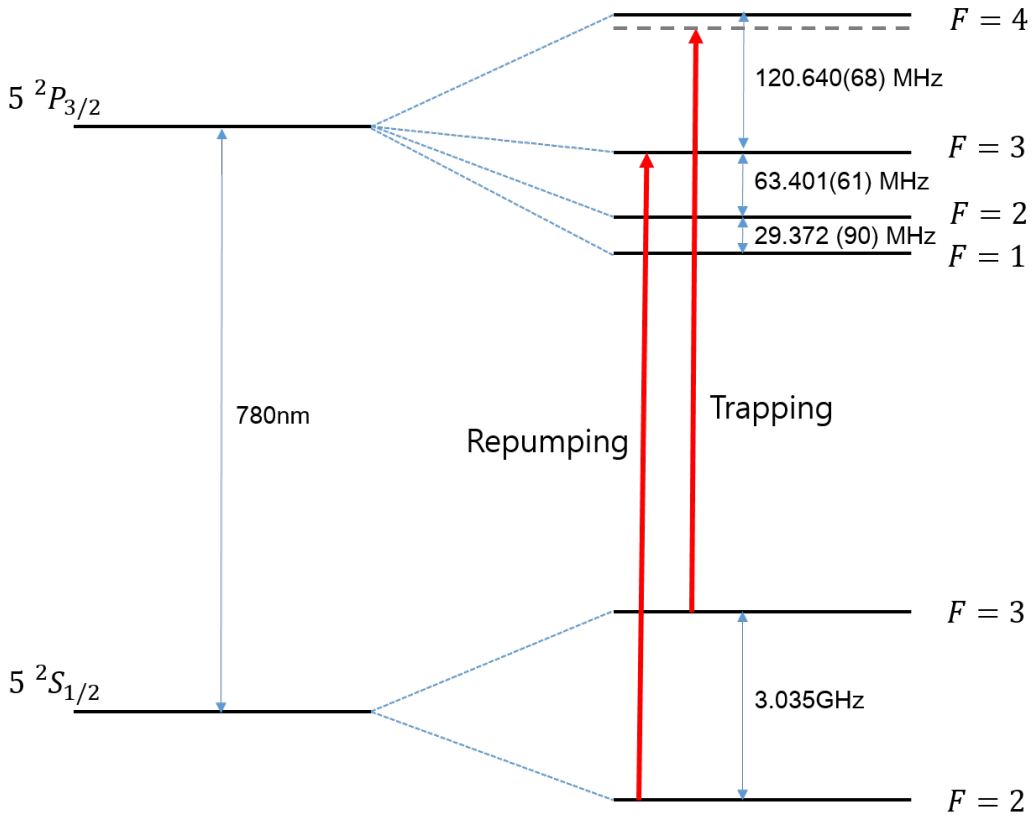

Figure 2.3: Rubidium 85 D2 transition hyperfine structure [5].

trum line of MTS and it is controlled finely by AOM. Since the MTS signal is more stable than SAS signal against the change of the external environment (temperature and the intensity of laser).

2.2.3 System Control

For obtaining the florescence images of trapped atoms, we use charge coupled device(CCD) camera which is controlled by the software program 'WinSpec32'. And we use the Labview program for control precisely the ND filter mounted

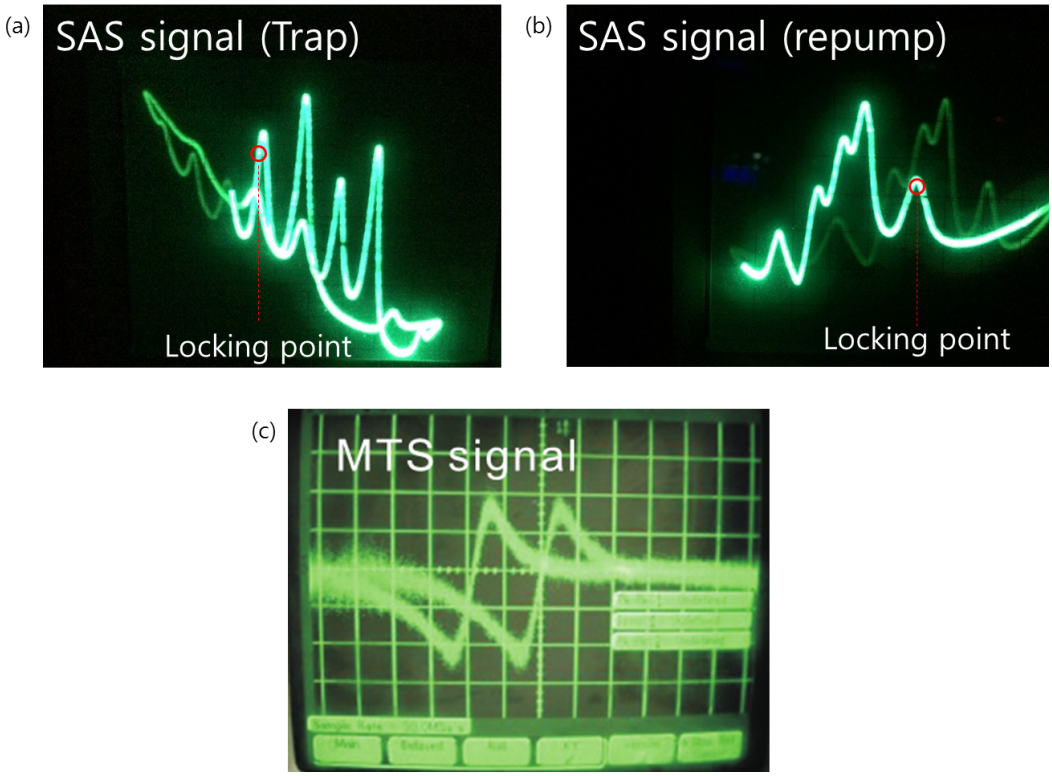

Figure 2.4: The saturated absorption spectroscopy (SAS) signal of (a) Trapping laser (b) Repumping laser and modulation transfer spectroscopy (MTS) signal of (c) Trapping laser.

to the stepper motor. By control the repumping laser of the system with ND filter, we adjust the total number of atoms. In addition, we improve the Labview program to be able to repeat the increasing and decreasing sequence in order. It was described in detail in the appendix. The manipulations of phase shift between the modulation signal of the left side of z-axis and the one of the other side of the z-axis, signal adding and switching are achieved by the handmade electronic circuit.

Bibliography

[1] Y. Kim, Ph. D. thesis, Seoul National University, 2011.

[2] G. Moon, Ph. D. thesis, Seoul National University, 2013.

[3] Christopher J. Foot, *Atomic Physics* (Oxford, New York, 2005).

[4] D. J. McCarron, S. A. King and S. L. Cornish, Meas. Sci. Technol. **19**, 105601.

[5] D. A. Steck, Rubidium 85 D Line Data, 2010.

[6] H. Metcalf and P. van der Stranten, *Laser Cooling and Trapping* (Springer, New York, 1999).

[7] K. Kim, H-R. Noh, Y-H. Yeon, and W. Jhe, Phys. Rev. A **68**, 031403 (2003).

[8] K. Kim, H-R. Noh, and W. Jhe, Opt. Comm. **236**, 349 (2004).

[9] M-S. Heo, Y. Kim, K. Kim, G. Moon, J. Lee, H-R. Noh, M. I. Dykman, and W. Jhe, Phys. Rev. E **82**, 031134 (2010).

Chapter 3

The Driven Cold Atom System

3.1 Parametrically Modulated MOT System

In our system, we restrict the movement of atoms in one dimension by the laser intensity of z-axis, the axis of the anti-Helmholtz coil, is enough weaker than the one of other axis. We can assume the two-level approximation in typical experimental conditions. The MOT equation of our system is

$$m\ddot{z} = \frac{\hbar k\Gamma}{2}\left[\frac{s_0}{1+s_0+\frac{4}{\Gamma^2}(\delta - k\dot{z} - \frac{\mu_B b}{\hbar}z)^2} - \frac{s_0}{1+s_0+\frac{4}{\Gamma^2}(\delta + k\dot{z} + \frac{\mu_B b}{\hbar}z)^2}\right], \tag{3.1}$$

where m is the mass of an ^{85}Rb atom, k is the wave vector, Γ is the decay rate of the excited state of the atom (=$2\pi\times$6.07 MHz for ^{85}Rb atom), μ_B is the Bohr magneton, δ is the detuning of the laser frequency relative to the atomic resonance frequency, and b is the magnetic field gradient. s_0 is the intensity of

the laser normalized to the saturation intensity I_s (=1.67 mW/cm^2 for cycling transition).

The equation (3.1) can be expanded in a power series of z and $\dot{z}$ when the value s_0 is enough small, then the equation is simply written by

$$\ddot{z} + \beta\dot{z} + \omega_0^2 z + A_0\omega_0^2\left(z + \frac{\beta}{\omega_0^2}\dot{z}\right)^3 = 0 \tag{3.2}$$

where ω_0 is the trap frequency, β is the damping coefficient, and A_0 is the nonlinear coefficient. These parameters are

$$\omega_0 = \sqrt{\frac{8k\mu_B b s_0(-\delta/\Gamma)}{m(1+4(\delta/\Gamma)^2)^2}}, \tag{3.3}$$

$$\beta = \frac{\hbar k}{\mu_B b}\omega_0^2, \tag{3.4}$$

$$A_0 = 8\left(\frac{\mu_B b}{\hbar\Gamma}\right)^2 \frac{4(\delta/\Gamma)^2 - 1}{(4(\delta/\Gamma)^2+1)^2}. \tag{3.5}$$

In order to obtain the parametrically driven nonlinear oscillator in our system, we modulated the intensity of trapping laser as near the twice of the trap frequency. Then, we observe the parametric resonance which has two identical atomic clouds with the phase difference of π. It was observed in our previous experiments [7,8]. And the schematic is in the Figure 3.1. We use the conventional six-beam MOT had a pair of counter-propagating and intensity-modulated trapping lasers along the anti-Helmholtz coil axis (z-axis) [7]. The magnetic field gradient b was 10 G/cm, and the trap laser intensity was about 0.294 mW/cm^2. The detunings were about -2.05Γ ($\Gamma = 2\pi \times 6.06$ MHz is the decay rate of the excited state of ^{85}Rb) in the z-axis and -2.32Γ in the x- and y-axes.

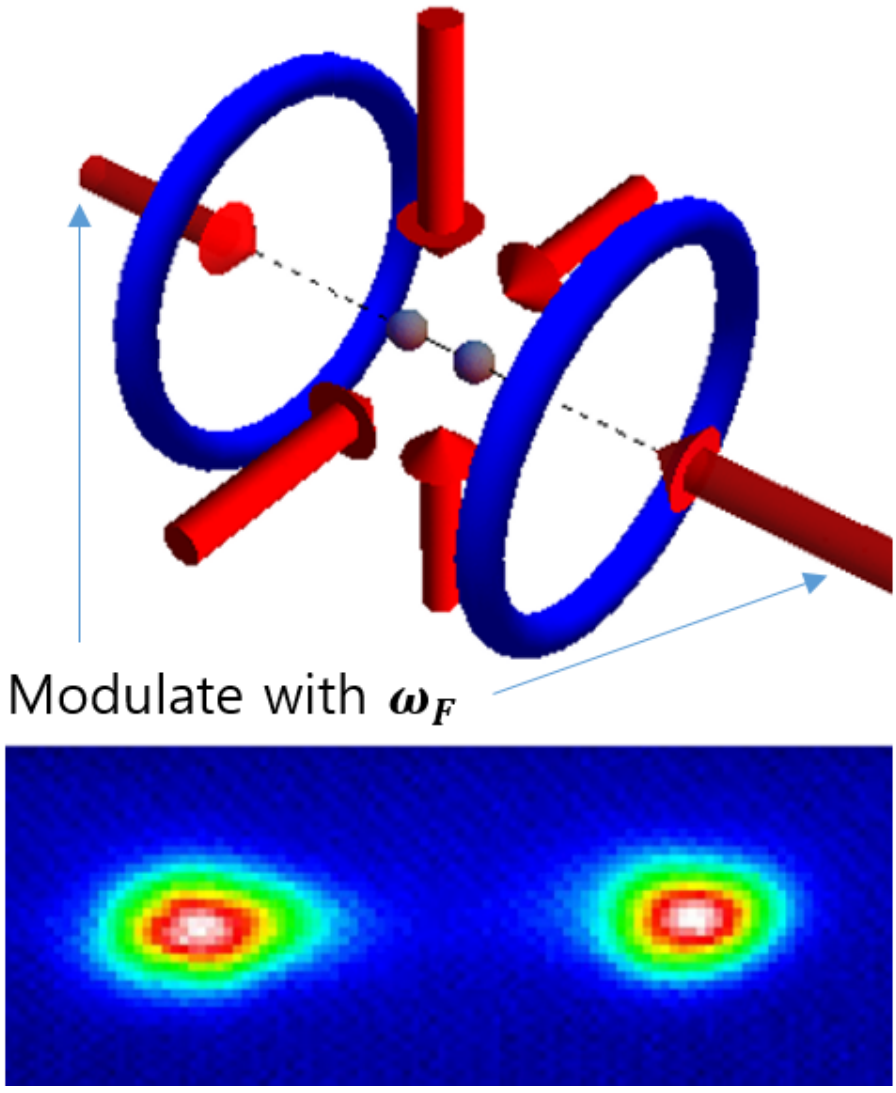

Figure 3.1: The schematic diagram of parametrically modulated MOT. The intensity of trapping laser on z-axis is modulated with modulation frequency ω_F and the system has two attractors.

The equation of motion of an atom in a parametrically modulated MOT, modifed form of Eq. (3.2) is given by

$$\ddot{z} + \beta\dot{z} + \omega_0^2(1 + \epsilon\cos\omega_F t)z + A_0\omega_0^2 z^3 = 0. \tag{3.6}$$

where ϵ is relative amplitude and ω_F is the modulation frequency.The equation of parametrically modulated MOT equation has two stable states in the rotating frame. Thus, the parametrically modulated MOT system has bistable states and a discrete time-translational symmetry with respect to time translation by the modulation period $\tau_F = 1/\omega_F$ as shown in the Fig. 3.2. But the period doubling does not break the time translation symmetry due to the fluctuations of the system. Even though the vibrational state by modulation has a lower asymmetry, the clouds are equally populated immediately by the fluctuations then, system remains symmetric state [1]. But, when the total number of atoms of the system increases and exceeds a certain number which is called the critical number the spontaneous symmetry breaking (SSB) transition occurs as shown in Fig. 3.2.

The SSB transition is originated from the light-induced interaction between two atomic clouds in this system. It is called shadow effect and it occurs because the one cloud which relatively has a large number of atoms obscures the laser from the other side of the atomic cloud. The atom on the side of less number of atoms moves toward the other side since the shadow effect as shown in Fig. 3.2. And we observe the SSB transition in a graph of the normalized number difference with the total number of atoms(Fig. 3.2). And the

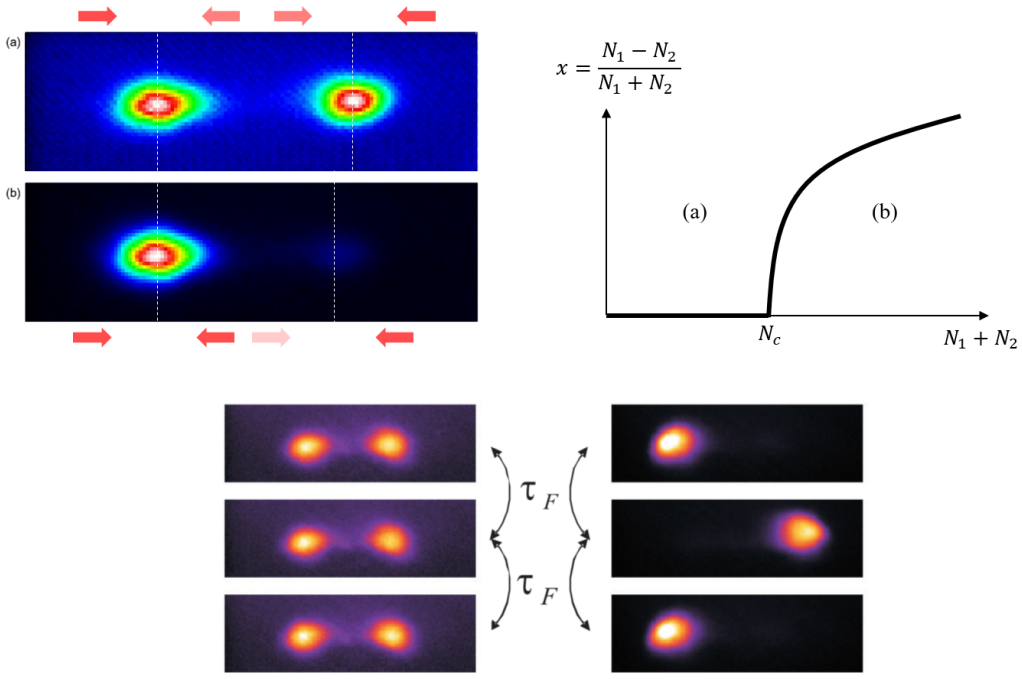

Figure 3.2: Typical images of spontaneous symmetry breaking transition and its graphs of the normalized number difference with the total number of atoms. The time-translational symmetry with respect to time translation by the modulation period τ_F and it changes to $2\tau_F$ when the symmetry breaking occurs [1].

critical exponents of transition, to characterize the universal class of that, are measured in our previous works [9]. The light-induced interatomic interaction which is called shadow force, the origin of SSB transition is described in detail in next section.

3.2 System Dynamics

3.2.1 Fluctuation-Induced Transtion

The present of noise enables the system to not infrequently overcome the activation barrier and switch between the bistable states. This transition has been studied in various system and it was described by Kramers' equation in equilibrium system [5, 10, 11]. In nonequilibrium system such as parametrically modulated system, theoretical calculating the transition rate was performed. The transition rate in many nonequilibrium systems was described by the similar form of the Kramers' equation [6, 7]. The noise-induced transition rate is important quantity to understand many phenomena related to the stochastic systems.

We measured the fluctuation-induced transition rate experimentally in our system [8]. It was done by emptying one of the two atomic clouds and measuring the subsequent recovery time of the empty one. For doing this, we used the additional bias field which was realized by bias modulation with half the parametric modulation frequency $\omega_F/2$. When we applied the bias field in the direction of one cloud, the cloud has most of the population. And the bias field was turned off suddenly, then two atomic clouds repopulated equally by the fluctuation-induced transition. We measure the repopulation time for transition rate. The transition rate is extracted from the decay of the number difference of the atomic clouds as shown in Fig. 3.3 (b).

$$N_1 - N_2 = N_0 \exp(-2Wt), \tag{3.7}$$

where N_1 and N_2 are the population of the each cloud, N_0 is the constant and W is the fluctuation-induced transition rate between two clouds. The measured transition rate W is 0.1 to 5 s^{-1} as the experimental parameters. In our system as shown in Fig. 3.3 (b), the obtained transition rate is about 0.31 s^{-1}.

Note that the transition rate W has the form similar to the Kramers' equation in equilibrium system,

$$W = C \exp(-R/D), \tag{3.8}$$

where C is the constant, D is the diffusion constant (or noise intensity) of the system, and R is the activation energy which corresponds to the height of the barrier of the potential in equilibrium systems. The activation energy R is the most important quantity to describe the system dynamics, and we give the theoretical analysis for the activation energy on our previous work by path-integral formalism [1].

3.2.2 Light-Induced Inter-atomic Interaction

The another dynamic of the system is inter-atomic interaction due to laser light. It comes from the shadow effect which is originated from shielding the laser light applied to the atoms by other atoms [9, 12]. The interaction is the long-range interaction and affects the switching rate between the atomic clouds. In the one-dimensional picture, the shadow force on ith atom with coordinate z^i due to other atoms can be approximately modeled as $F^i = -f_{\rm sh} \sum_j \mathrm{sgn}(z^i - z^j)$

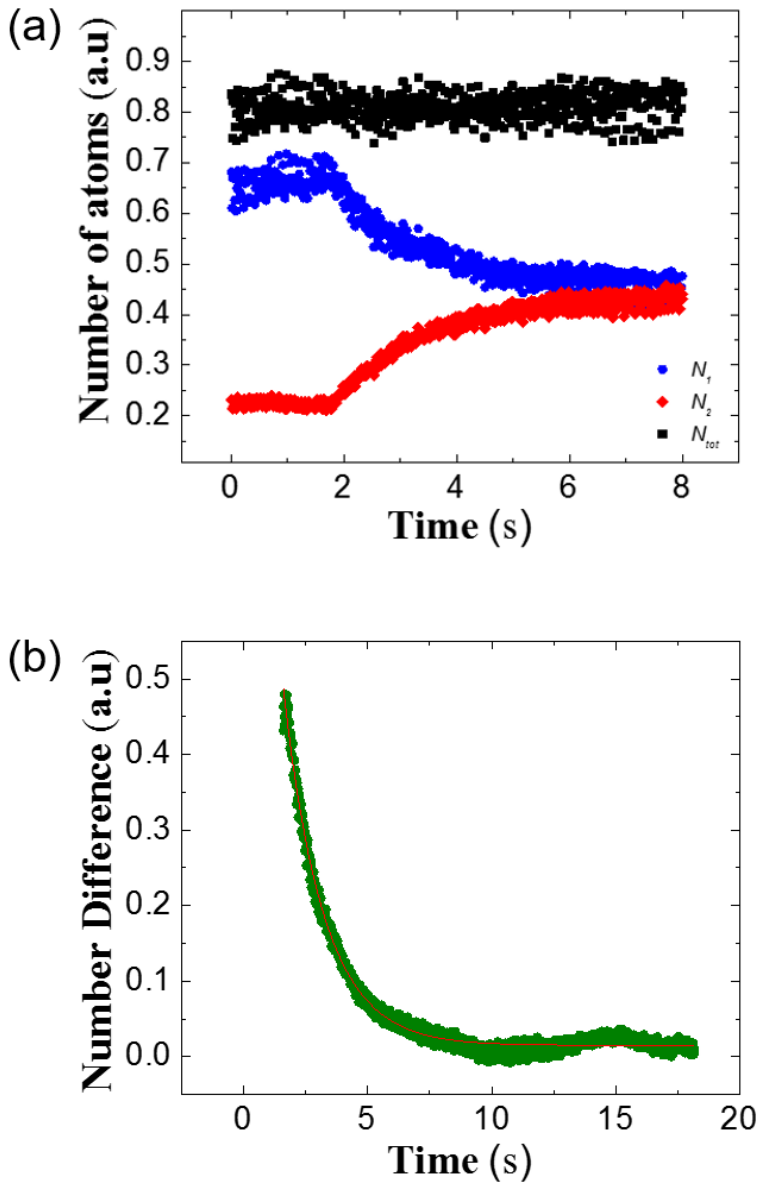

Figure 3.3: Typical data of the fluctuation-induced transition (a) Time evolutionn of the atomic clouds after bias field is turned off (b) The decay of number difference of two atomic clouds.

as shown in Fig. 3.4 [1], where f_{sh} is the shadow force due to a single atom. This force is weak, much smaller than the Doppler force that might not be atoms to escape from the trap. But the shadow force affects the activation energy and compels the atoms to move toward the more populated atomic clouds. In other words, the interaction acts to break up the symmetry of the system.

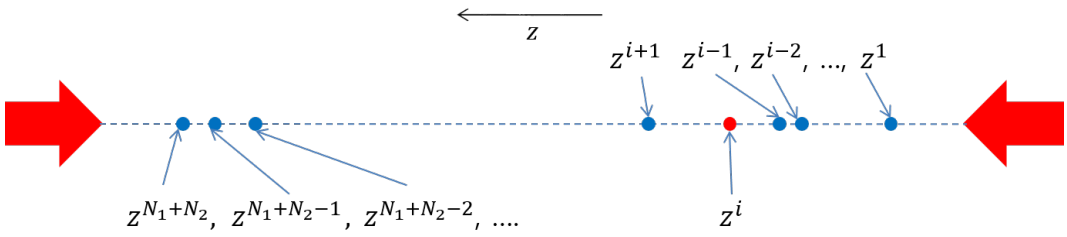

Figure 3.4: The one-dimensional model of the shadow force.

When the system has slight number difference, the fluctuation-induced transition plays a role of keeping the symmetry of two atomic clouds. By the competition of the noise-induced transition and the inter-atomic interaction, the symmetry breaking transition is determined that it occurs or not. At below the critical number of atoms, the fluctuation-induced transition is dominant. But when the total number of atoms exceeds the critical number, the inter-atomic interaction is dominant. Thus the spontaneous symmetry breaking transition occurs in this condition. The fluctuation-induced transition and the inter-atomic transition can be analogous as the thermal fluctuation and spin interaction in the magnet system. The shadow effect is a real force, the not just model then, the shadow force can be measured. Since the force is very weak and collective behavior of atoms, it is difficult to quantitatively analyze. But the experimental

measurement of the magnitude of the shadow force and description in detail are in our previous works [9].

3.3 Response to the Number Sweeping

In the spontaneous symmetry breaking (SSB) transition, the transition occurs as increasing the total number of atoms. When the total number of atoms exceeds ,the critical number the order parameter of this transition, the normalized number difference has a non-zero value and increase also as shown Fig. 3.2. And it is the stationary solution of the SSB transition. A hysteresis occurs when the total number of atoms changes with time. We observe the hysteresis of SSB transition by sweeping the total number of atoms uniformly in our system as shown in Fig. 3.5. We observe that the transition points of increasing and decreasing case shift from the critical point of the stationary solution. It is originated from the critical slowing down near the critical point. The specific discussion of the critical slowing down phenomena is explained in next section.

3.3.1 Analogy of the SSB transition

The spontaneous symmetry breaking (SSB) transition can be analogous as the ferromagnetic-paramagnetic transition as shown in Fig. 3.6. At high temperature, in other words, when the temperature of the system is above the Curie temperature, the thermal energy of magnet system is larger than the interaction between spins thus, the high thermal energy interrupts the align of spin by spin

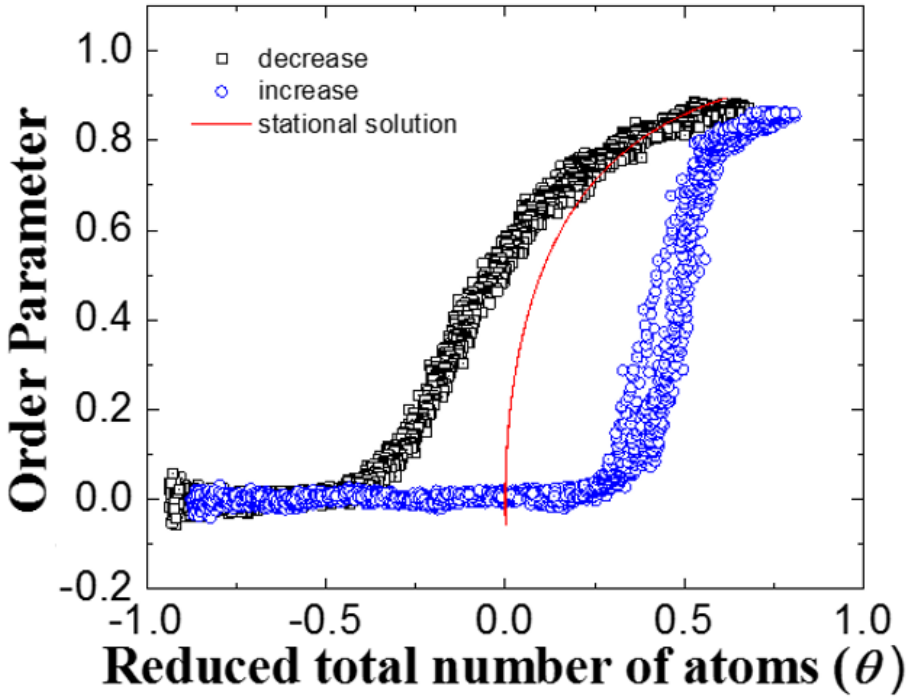

Figure 3.5: The hysteresis in the spontaneous symmetry breaking transition by number sweeping. The sweeping rate is 1.87×10^6 s^{-1}.

interaction [13]. It is called paramagnetic state. This is similar to the situation that keeping the symmetry of system by the noise-induced transition although the system has slight number difference at below critical number. Contrariwise, when the temperature of magnet system is below Curie temperature, the spins of the system are aligned by the spin interaction which is lager than thermal energy and it is called ferromagnetic state. It is similar to the symmetry breaking state of our system at above critical number. In this state, inter-atomic interaction is dominant. Therefore, lowering the temperature in the magnet system can be similar to the increasing the number of atoms in our system effectively and vice versa.

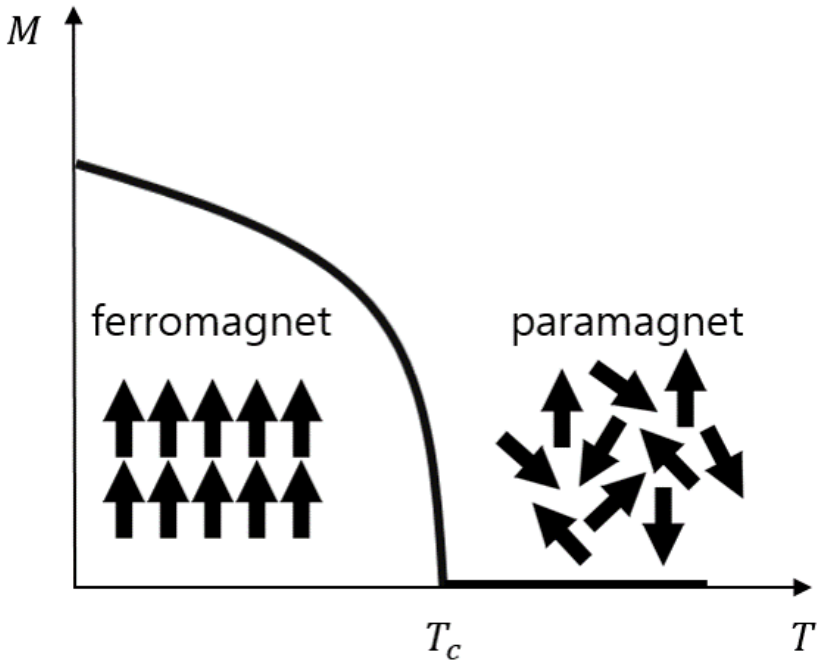

Figure 3.6: The paramagnetic to ferromagnetic phase transition in the magnet system. It can be analogous with symmetry breaking transition in our system.

Bibliography

[1] Y. Kim, Ph. D. thesis, Seoul National University, 2011.

[2] K. Kim, H-R. Noh, Y-H. Yeon, and W. Jhe, Phys. Rev. A **68**, 031403 (2003).

[3] K. Kim, H-R. Noh, and W. Jhe, Opt. Comm. **236**, 349 (2004).

[4] M-S. Heo, Y. Kim, K. Kim, G. Moon, J. Lee, H-R. Noh, M. I. Dykman, and W. Jhe, Phys. Rev. E **82**, 031134 (2010).

[5] W. Horsthemke and R. Lefever, *Noise-Induced Transtions* (Springer-Verlag, Berlin, 1982).

[6] L. I. McCrann, M. I. Dykman, and B. Golding, Nature **402**, 785 (1999).

[7] J. Haled, A. Zhukov, R. Roy, and M. I. Dykman, Phys. Rev. Lett. **85**, 78 (2000).

[8] M. I. Dykman, C. M. Maloney, V. N. Smelyanskiy, and M. Silverstein, Phys. Rev. E **57**, 5902 (1998).

[9] M. I. Dykman *et al.*, International Journal of Bifurcation and Chaos, **8**, 747 (1998).

[10] K. Kim, M-S. Heo, K-H. Lee, H-J. Ha, K. Jang, H-R. Noh, and W. Jhe Phys. Rev. A **72**, 053402 (2005).

[11] T. Walker, D Sesko, and C. Wieman, Phys. Rev. Lett. **64**, 408 (1990).

[12] A. M. Steane, M. Chowdhury, and C. J. Foot, J. Opt. Soc. Am. B **9**, 2142 (1992).

[13] Ch.V. Mohan, M. Seeger, H. Kronmüller, P. Murugaraj, and J. Maier, J. Mag. Mag. Mat. **183**, 348 (1998).

Chapter 4

Critical Slowing Down: Cause of the Hysteresis

4.1 Introduction

The critical slowing down is a critical phenomenon of the phase transition. To understand the slowing down we consider a ball in a well as shown in Fig. 4.1. The ball represents a state of the system and the well represents the potential of the system. When the ball is perturbed by changing of external conditions, it recovery own state relatively fast from the perturbated state in far from transition point. As the system approaches the transition point, the width and stiffness of the well become lower [1]. It means that the transition happens easily by perturbation. Thus, the recovery time of the state of the system from perturbed state to equilibrium state becomes longer, when the state of the system ap-

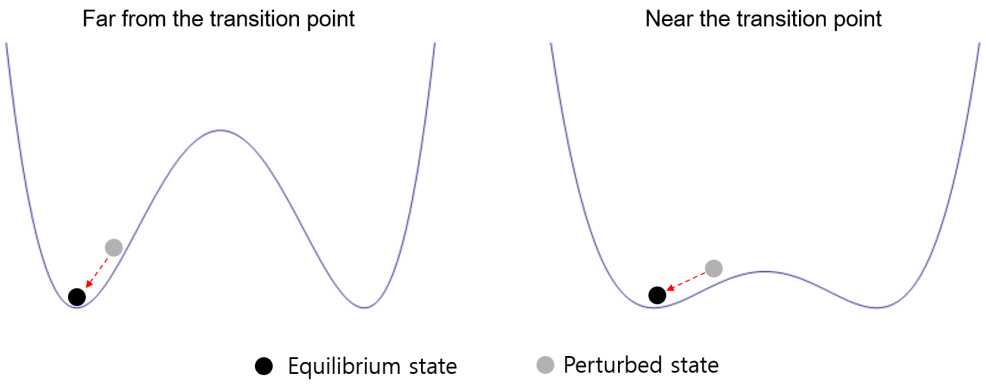

Figure 4.1: A illustration of the crtical slowing down phenomena.

proaches the point of transition. We theoretically describe the critical slowing down and obtain the relaxation times at each point of system experimentally in next section.

4.2 Theoretical Description

4.2.1 The Mean-Field Equation of Motion of Order Parameter

The SSB transition originates from the light-induced long range interaction which is called shadow force, due to the shielding effect of atoms from the laser light by other atoms [2, 3]. Hysteresis loops are observed with a constant sweeping rate of a total number of atoms. In one-dimensional approximation the force, exerted on one atom at the coordinate z^i from other atoms, can be described as $F^i = -f_{\mathrm{sh}} \sum_j \mathrm{sgn}\,(z^i - z^j)$ where f_{sh} is a constant representing the

shadow force due to the single atom [4] and it is a value related to critical number of atom in this system. In order to theoretically describe the symmetry breaking transition with sweeping of total number of atoms, the dynamic evolution of the two clouds having respectively N_1 and N_2 atoms can be found from the following master equations:

$$\frac{dN_1(t)}{dt} = -W_{12}N_1(t) + W_{21}N_2(t) + \frac{R}{2}, \tag{4.1}$$

$$\frac{dN_2(t)}{dt} = -W_{21}N_2(t) + W_{12}N_1(t) + \frac{R}{2}, \tag{4.2}$$

where

$$W_{ij} \equiv W_0 \exp\left[-\lambda \frac{N_i - N_j}{N}\right] \tag{4.3}$$

are the transition rates between the two clouds and the indices i, j are 1 or 2, W_0 is the transition rate without additional modulation. We note that $N = N_1 + N_2$ is the total number of atoms. $\lambda \equiv \theta + 1 = N/N_c$ represents the normalized total number of atoms where N_c is the critical number of the SSB transition and θ is the reduced total number of atoms. R is the sweeping rate of the total number of atoms.

Solving Eqs. (4.1) and (4.2) for the normalized number difference between the two clouds, $x = (N_1 - N_2)/N$, which corresponds to the order parameter of the SSB phase transition, we obtain:

$$\frac{d(N_1 - N_2)}{dt} = -2W_{12}N_2 + 2W_{21}N_1. \tag{4.4}$$

Divided by total number N both side

$$\frac{dx}{dt} = 2W_{12}[-\frac{N_1}{N} + \frac{N_2}{N}], \tag{4.5}$$

where

$$\frac{N_1}{N} = \frac{(1+x)}{2} \tag{4.6}$$

$$\frac{N_2}{N} = \frac{(1-x)}{2}. \tag{4.7}$$

the Eq. (4.5) becomes

$$\frac{dx}{dt} = 2W_0[-\frac{(1+x)}{2}\exp(-\lambda x) + \frac{(1-x)}{2}\exp(\lambda x)]. \tag{4.8}$$

then the mean-field equation of motion of order parameter is gvien by

$$\frac{1}{2W_0}\frac{dx}{dt} = -x\cosh[(\theta+1)x] + \sinh a[(\theta+1)x]. \tag{4.9}$$

Since the total number was swept with a uniform rate, the total number of atoms becomes a function of time. Thus, the reduced number can be written as $\theta(t) = \theta_0 + R't$ where $R' = R/N_c$. When the total number of atoms is changed with time, the light-induced inter-atomic interaction caused by shadow force is changed in accordance with the total number of atoms as well. Due to this variation of the interaction, the order parameter relaxes toward a new equilibrium state which is appropriate to the total number of atoms at that time. This relaxation time is expected to become larger when the total number approaches the critical number. When the reduced number of atoms θ is a function of time, the numerical results of the Eq. 4.9 are shown in Fig. 4.2.

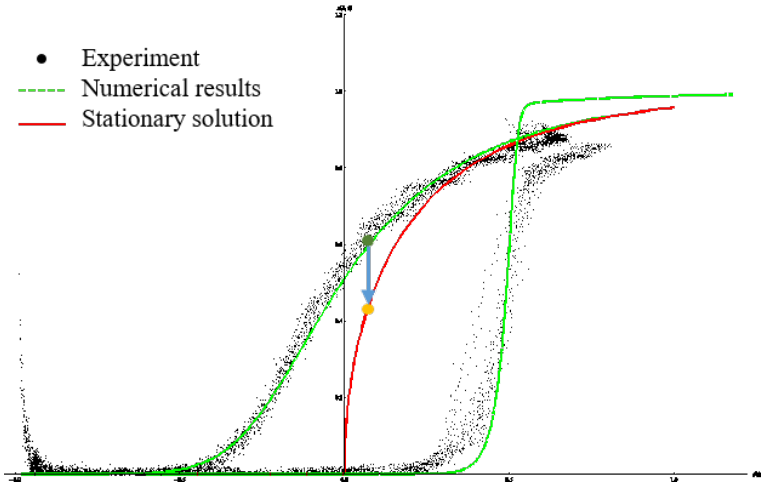

Figure 4.2: The numerical results of mean-field equation of motion with experiments. After stopping sweeping number of atoms at some point, the order parameter of transtion relaxes to the state of stationary solution.

4.2.2 Relaxation Time

In order to obtain the relaxation time at some point of reduced total number of atoms, we expand right-hand side of Eq. (4.9) about the point $x = x_s$ [5] and the reduced total number of atoms becomes a constant since the number sweeping stopped. At $\theta < 0$, i.e. $N < N_c$, x_s=0, Eq. (4.9) becomes

$$\begin{aligned} \eta \frac{dx}{dt} &\cong -x + (\theta + 1)x \\ &= \theta x, \end{aligned} \tag{4.10}$$

but $\theta < 0$,

$$\eta \frac{dx}{dt} \cong -|\theta|\, x. \tag{4.11}$$

And thus, the order parameter is given by

$$x = x_0 \exp\left[-\frac{|\theta|\, t}{\eta}\right], \tag{4.12}$$

where $\eta = 1/(2W_0)$, and $x_0 = x(t=0)$. The obtained result of order parameter means that it exponentially decay with time evolution. When $\theta > 0$, i.e. $N > N_c$, $x_s = \tanh a[(\theta+1)x_s]$. Then, we can expand Eq. (4.9) about x_s up to the first order in $x - x_s$ as

$$\begin{aligned}\eta\frac{dx}{dt} \cong & -x_s \cosh\left[(\theta+1)x_s\right] \\ & - \left(\cosh\left[(\theta+1)x_s\right] + (\theta+1)x_s \sinh\left[(\theta+1)x_s\right]\right)(x - x_s) \\ & + \sinh\left[(\theta+1)x_s\right] + (\theta+1)\cosh\left[(\theta+1)x_s\right](x - x_s) \end{aligned} \tag{4.13}$$

from the stationary solution $x_s \cosh[(\theta+1)x_s] = \sinh[(\theta+1)x_s]$. Then Eq. (4.13) can be written by

$$\eta\frac{dx}{dt} \cong -\left[1 - (\theta+1)(1-x_s^2)\right]\cosh a\left[(\theta+1)x_s\right](x - x_s) \tag{4.14}$$

The solution of Eq. (4.14) is simply given by

$$x = (x_0 - x_s)\exp\left[-\frac{\epsilon}{\eta}t\right] + x_s, \tag{4.15}$$

where $\epsilon = [1 - (\theta+1)(1-x_s^2)]\cosh\left[(\theta+1)x_s\right]$.

And this result represents that the order parameter exponentially decays with time and converge to the stationary solution of the order parameter. In Figure 4.3, we obtained the time evolution of the order parameters after stopping number sweeping. The order parameter exponentially decays with time as we expected and the time constants of a solution of the order parameter becomes longer as shown in Fig. 4.3.

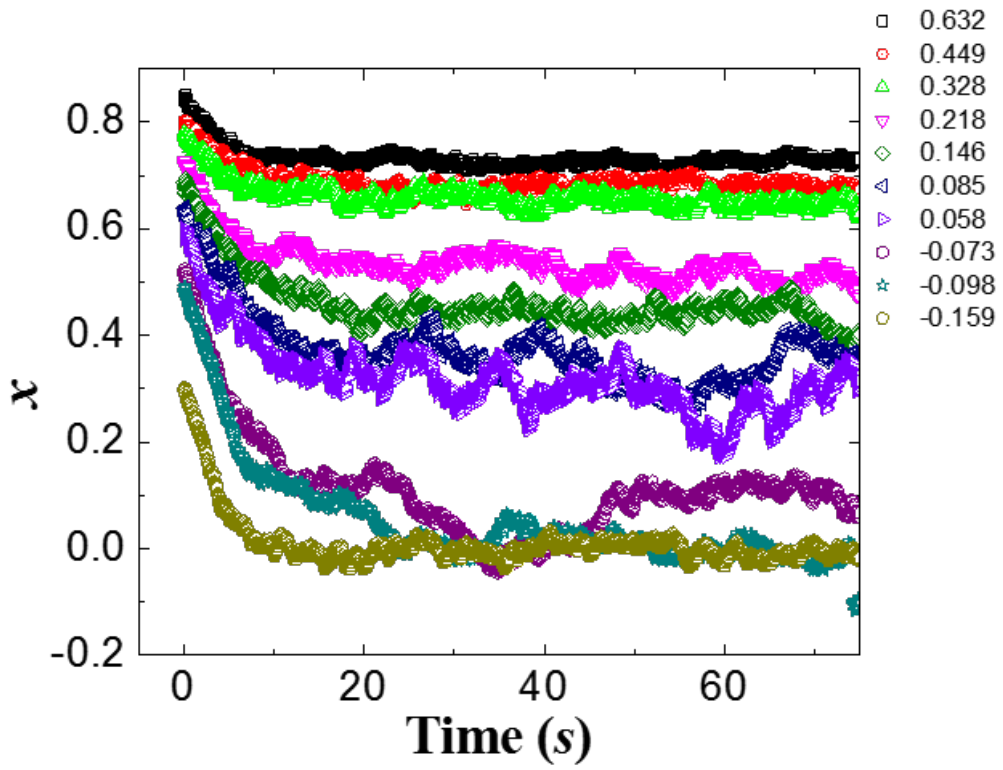

Figure 4.3: Time evolution of the order parameter after stopping number sweeping at each points of the reduced total number.

Finally, the relaxation time τ is obtained as follows:

$$\tau = \begin{cases} \frac{\eta}{|\theta|}\,, & \text{for } \theta < 0\,, \\ \\ \frac{\eta}{\epsilon}\,, & \text{for } \theta > 0\,. \end{cases} \tag{4.16}$$

It is expected to increase when the reduced total number of atoms approaches the critical point.

4.3 Experimental Methods

The parameters of the system, the laser condition and magnetic field are same as the description in chapter 2. For measuring the relaxation time, we obtain the time evolution of the order parameter Immediately after stopping sweeping the number of atoms. The sweeping rate is fixed as 3.72×10^6 s^{-1}, This is an expected value when the pulse interval of stepper motor is 5ms. And the values of the result were the average of the performed experiments over more than three times. The evolution times of the order parameter were enough long that the order parameter approaches the equilibrium.

4.4 Experimental Results and Discussion

We obtained relaxation times experimentally by measuring the time that the order parameter has been stabilized to the steady state when stopping changing the number of atoms at some points during the process of number sweeping as

shown in Fig. 4.3. And the Figure 4.4 shows the measured relaxation time at various reduced numbers of atoms with sweeping rate $R = 3.72 \times 10^6$ s^{-1}. As can be seen in Fig. 4.4, the relaxation time increases as the reduced total number of atom approaches toward the critical number of the phase transition and diverges at the critical point $\theta = \theta_c (= 0)$ as expected. In Fig. 4.4, the red solid curves represent the solutions of Eq. (4.16). The difference between numerical results and experimental data is originated from high order term of expansion of Eq. 4.9 at both side. But numerical results and experimental data are consistent well near the critical number of the transition. Furthermore, Since the relaxation time increase when the system approaches critical point, It is considered to be sufficient as proof of the slowing down.

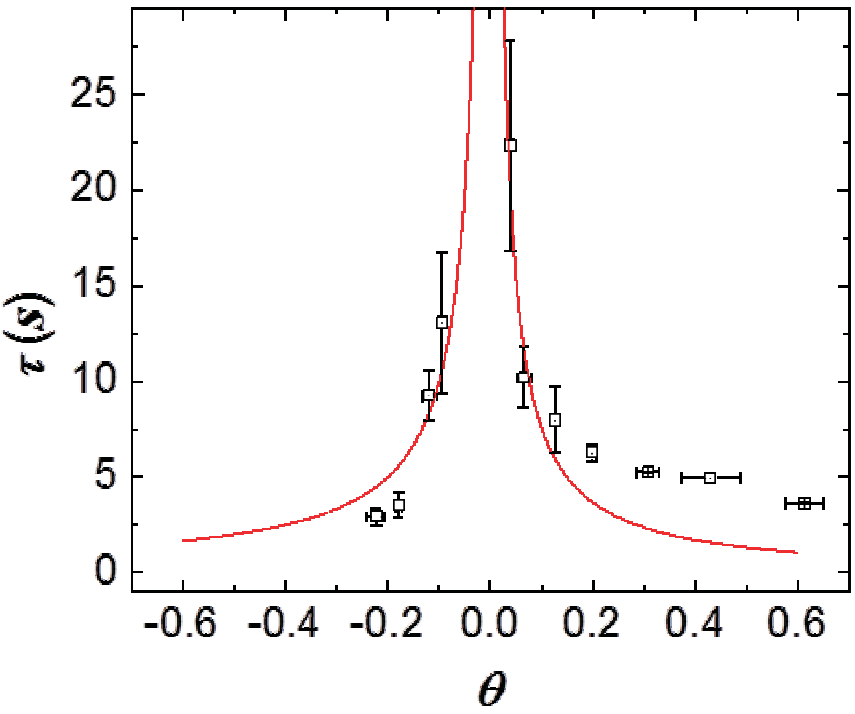

Figure 4.4: Measured relaxation times to the equilibrium state at each reduced number superimposed with numerical results of Eq. (4.16) with $N_c = 4.81 \times 10^7$ and $R = 3.72 \times 10^6$ s^{-1}.

Bibliography

[1] I. A. van de Leemput *et al.*, PNAS **111**, 87 (2014).

[2] T. Walker, D. Sesko, and C. Wieman, Phys. Rev. Lett. **64**, 408 (1990).

[3] D. W. Sesko, T. G. Walker, and C. E. Wieman, J. Opt. Soc. Am. B **8**, 946 (1991).

[4] M. S. Heo, Y.H. Kim, K. Kim, G. Moon, J. Lee, H.R. Noh, M. I. Dykman, and W. Jhe, Phys. Rev. E. **82**, 031134 (2010).

[5] A. Misra and B. K. Chakrabarti, Phys. Rev. E. **58**, 4277 (1998).

[6] K. Kim, M-S. Heo, K-H. Kim, H-J. Ha, K. Jang, H-R. Noh, and W. Jhe, Phys. Rev. A **72**, 053402 (2005).

Chapter 5

Scaling Behavior of the Hysteresis

5.1 Introduction

Hysteresis, one of non-equilibrium phenomena with varying temperature of system, is one of the most interesting topics that have been studied in various fields such as molecular switching using spin crossover [8–10], temperature driven metal-insulator transition (MIT) in solid state devices [5, 11], and antifreeze proteins (AFPs) in bionic system [6, 7]. The phenomenon of thermal hysteresis was reported in mean-field model [8].

In this model the closed hysteresis loop area (A) scales with a rate of temperature R as

$$A = A_0 + bR^n, \tag{5.1}$$

where n is the scaling exponent of the hysteresis and A_0 and b are constants. It is known that n approaches two-thirds which is universal for both the mean-field and field theoretical models concerned [8, 9].

In this thesis, we observed a hysteretic behavior of spontaneous symmetry breaking (SSB) transition in the modulated atomic system by sweeping the total number of atoms linearly. We determined the universality class of the hysteresis by obtaining the scaling exponent of hysteresis loops. First, we analyze theoretical description for determining the class of hysteresis in next section. We discuss the scaling behavior of the hysteresis and physical meaning also

5.2 Modeling of the Hysteresis with Mean-field Theory

In order to identify the class of the hysteresis in our system, we analyze the SSB transition. When the trapped numbers of the two atom clouds of parametrically modulated MOT are N_1 and N_2, the probability of system which describes the many-body system since it has above 10^7 atoms, $P_1(N_1)$ can be obtained from the following master equation [10]:

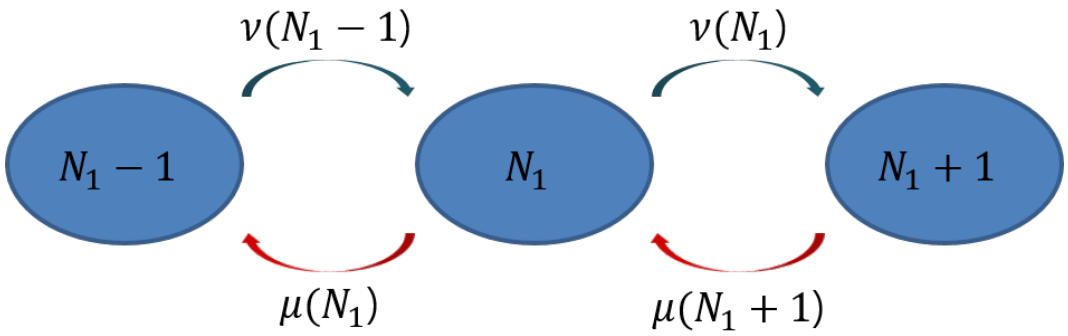

Figure 5.1: A schematic of the master equation in parametrically modulated MOT system.

$$\begin{aligned}
\dot{P}_1\Upsilon(N_1) &= -\left[\mu(N_1)+\nu(N_1)\right]P_1(N_1) \\
&\quad +\nu(N_1-1)P_1(N_1-1) \\
&\quad +\mu(N_1+1)P_1(N_1+1), \\
\mu(N_1) &= N_1 W_{12}(N_1;N), \\
\nu(N_1) &= (N-N_1)W_{12}(N-N_1;N).
\end{aligned} \tag{5.2}$$

The stationary solution of Eq. (5.2) is becomes

$$P_1^{\mathrm{st}}(N_1) = P_1^{\mathrm{st}}(0)\sum_{N=1}^{N_1}\frac{\mu(N-1)}{\nu(N)}. \tag{5.3}$$

$$P_1^{\mathrm{st}}(N_1) = Z^{-1}\begin{pmatrix} N \\ N_1 \end{pmatrix}\exp\left[-2\alpha N_1(N-N_1)\right], \tag{5.4}$$

where Z is a normalization constant, $\alpha = N_c \propto f_{\mathrm{sh}}/T$, and T is temperature of the system.

The reduced difference of the cloud populations, i.e., the order parameter of the phase transition, is determined theoretically by the maximum of the stationary solution $P_1^{\rm st}\ (N_1)$ [10]. For $x = (N_1 - N_2)/N \ll 1$, the probability is given by:

$$\begin{aligned} P_1^{\rm st}(N_1) &\cong Z^{-1} \exp\left[-N\left(x^4 - 6(\alpha N - 1)x^2\right)/12\right] \\ &= Z^{-1} \exp\left[-N\left(\frac{1}{12}x^4 - \frac{1}{2}\theta x^2\right)\right], \end{aligned} \tag{5.5}$$

where $\alpha = 1/N_c$ and $\theta = N/N_c - 1$. If the Landau type free energy per single atom of the system is defined by $L \equiv x^4/12 - \theta x^2/2$, it has an analogous form with the free energy of mean-field model as [11]

$$F = \frac{1}{2}rM^2 + \frac{1}{4}uM^4 + \frac{1}{6}vM^6 - HM, \tag{5.6}$$

where r is the reduced temperature with respect to the critical temperature, u, v are parameters, and H is the external field. In our case the sixth power term in Eq. (5.6) is negligible and H is zero. Thus, the parameter θ plays a role of reduced temperature which is the deviation from the critical temperature and is the control parameter. In contrast, x plays a role of the order parameter in the phase transition [10]. Therefore, the hysteresis of SSB transition which occurs by the total number sweeping has an analogy with the thermal hysteresis in other systems.

When the reduced total number of atoms (θ) is negative, the solution has one maximum at $x = 0$, and it has two maxima when θ is positive [10]. They are described by the following equation:

$$x = \tanh a\left[(\theta + 1)x\right], \tag{5.7}$$

that generates the red solid curves in Fig. 5.3.

5.3 Experimental Methods

The experimental setup of the system is described in detail in chapter 2. The magnetic field gradient b was 10 G/cm, and the trap laser intensity was about 0.294 mW/cm^2. The detunings were about -2.05Γ ($\Gamma = 2\pi \times 6.06$ MHz is the decay rate of the excited state of ^{85}Rb) in the z-axis and -2.32Γ in the x- and y-axes.

The modulation frequency of the trapping laser along the z-axis is twice of the trap frequency in the same direction and it can be adjusted by the function generator. In this experiment, the modulation frequency is $\omega_F \cong 2\pi \times 150Hz$, and the modulation amplitude was about $\epsilon \cong 0.9$.

We sweep the total number of atoms by control the intensity of repumping laser of the system with ND filter and it was changed linearly in time as shown in the Fig. 5.2. For changing the sweeping rate, we adjust the pulse interval of each step of the stepper motor (5ms-65ms). The different area of hysteresis loop is due to the different sweeping rates. The calculation of loop areas using the mensuration by parts method is described in detail in the following appendix.

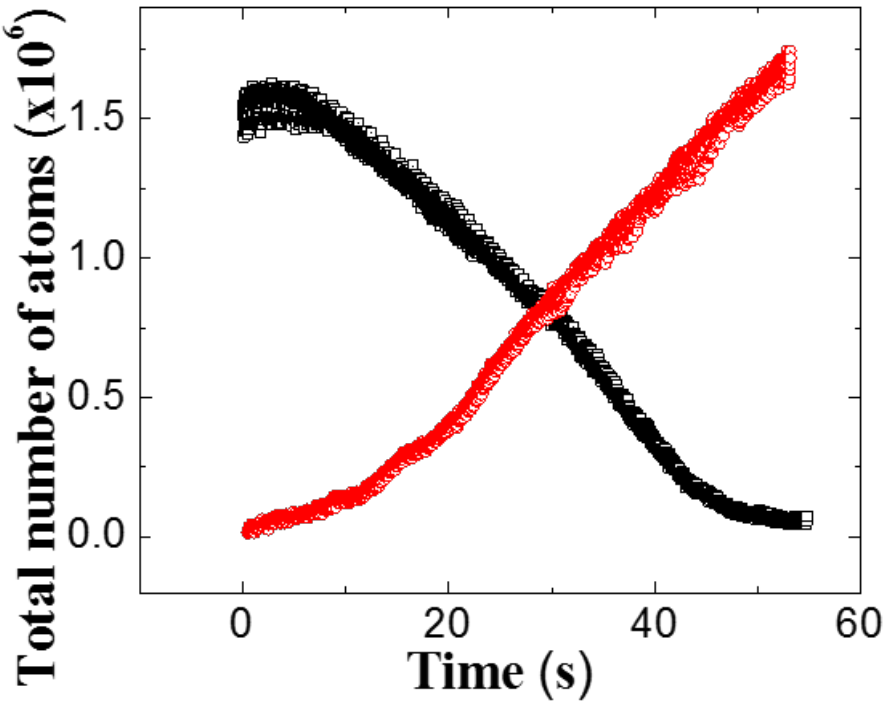

Figure 5.2: The number of atoms increases and decreases linearly in time.

5.4 Experimental Results and Disscusion

Figure 5.3 shows the hysteresis curves as a function of the reduced atom number with each sweeping rate of (a) 1.87×10^6 s^{-1}, (b) 9.61×10^5 s^{-1}, (c) 5.84×10^5 s^{-1}, and (d) 5.7×10^5 s^{-1}. The red curves in the Fig. 5.3 are the results calculated numerically from Eq. (5.7). The parameters, θ_c^i and θ_c^d are critical values of the reduced number for the symmetric state to the SSB state transition (upon increasing) and SSB state to Symmetric state transition (upon decreasing), respectively. The shadow effect, which is the cause of the SSB transition, does not

catch up with the variation of the number difference between the two clouds because the time of order parameter to relax toward the equilibrium state becomes larger and larger when the number of atoms approaches the critical point. Thus, when the total number of atoms is swept across the critical number with a uniform speed, the hysteresis loops can be obtained during the transition as shown in Fig. 5.3. It can be seen that the area of the hysteresis loop decreases as the sweeping rate of the total number of atoms is decreased.

Figure 5.4 (a) presents the scaling behavior of hysteresis loop areas versus the sweeping rate (R) of the total number of atoms on the log-log scale. Each points in Fig. 5 was obtained by averaging the experimental values more than three times and the constant term A_0 was derived by a linear fitting the plot of the hysteresis area A versus the sweeping rate R. The scaling exponent n in our system is 0.64 ± 0.04 which is quite close to the value given in the mean field theory [8]. Therefore, it is clearly seen that the hysteresis by the number sweeping in modulated MOT system exhibits a thermal hysteretic behavior. We define the hysteresis width as $\Delta\theta = \left|\theta_c^i - \theta_c^d\right|$. It is well known that the hysteresis width is consistent with the following scaling law

$$\Delta\theta \cong R^{\beta}, \tag{5.8}$$

where β is a scaling exponent [11]. The scaling exponent can be obtained by fitting the hysteresis width data to the double logarithmic form in Eq. (5.8). Log-log plot of the width of hysteresis $\Delta\theta$ versus sweeping rate R is shown in Fig. 5.4 (b). The scaling exponent (β) of hysteresis width in this work was found

to be 0.44 ± 0.025. This value is very close to the value predicted by the theory of the kinetic Ising model, which is 0.465 [12].

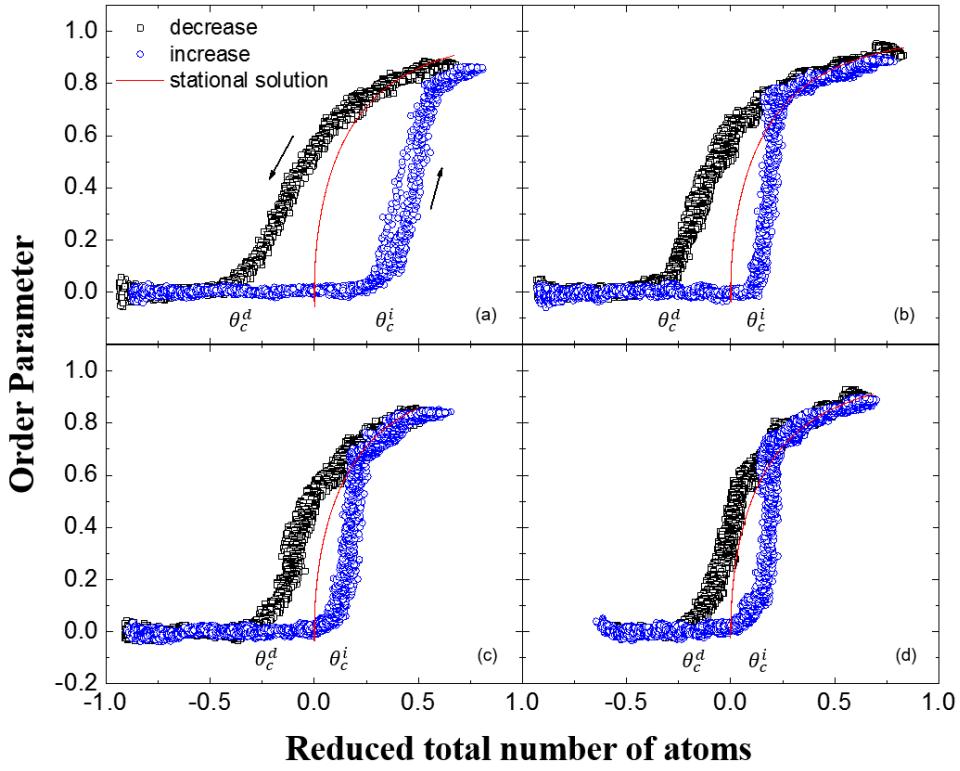

Figure 5.3: Measured hysteresis loops for various sweeping rates (pulse intervals). (a) 1.87×10^6 s^{-1} (10 ms) (b) 9.61×10^5 s^{-1} (20 ms), (c) 5.84×10^5 s^{-1} (30 ms), and (d) 5.7×10^5 s^{-1} (40 ms). The red solid curves are the solutions of Eq. (5.7).

5.5 Conclusion

Following the scaling theory of thermal hysteresis by Zhong et al. in Ref. [8], the scaling exponent of hysteresis width should have the physical meaning of resistance characteristics in the glass transition and coercivity in the spin transition. It means that ability of the system to withstand against the external stimulus without internal changes. Especially, to describe resistance of the system it should be compared with the exponent n reported in mean-field model [8,9,13]. The obtained value in our system is $\beta \sim 0.44 \pm 0.025$, which is smaller than the scaling exponent n in the mean-field model. This implies that our system is a model which has a rather low resistance.

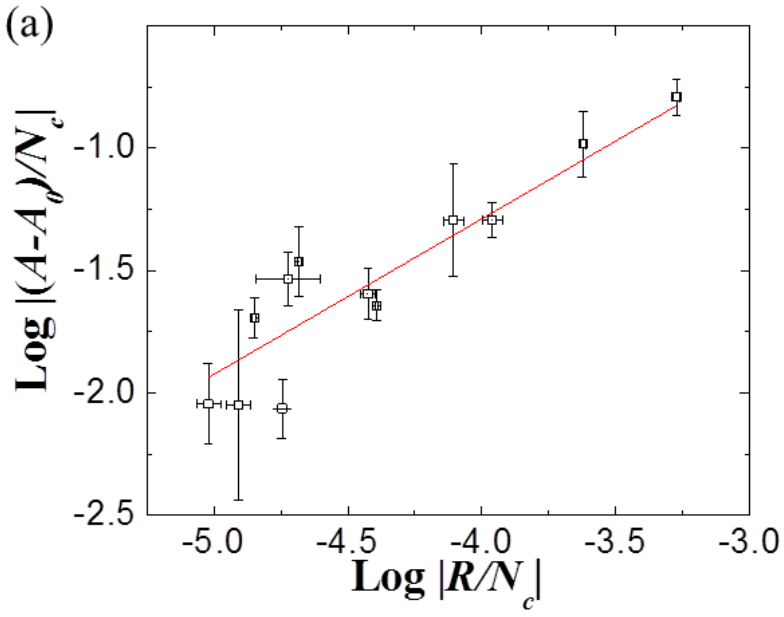

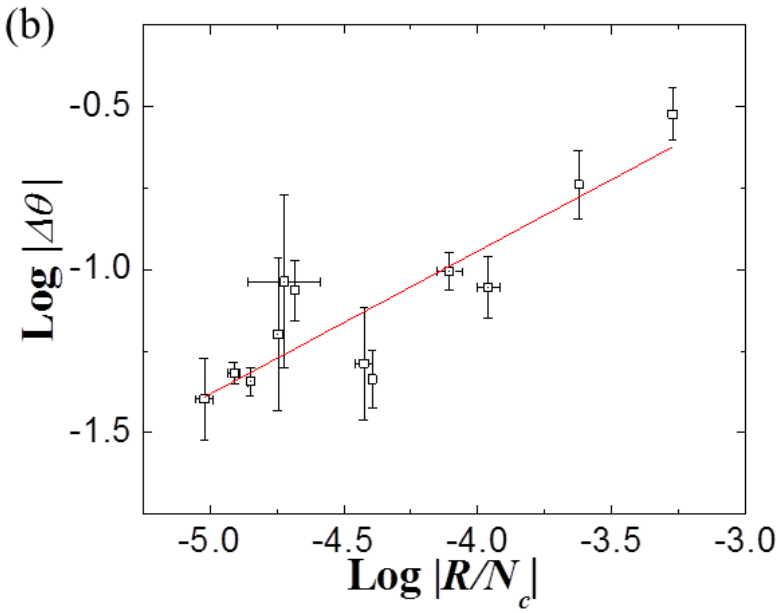

Figure 5.4: Log-log plot of (a) the hysteresis area A and (b) the hysteresis width $\Delta\theta$ versus number sweeping rate R. The solid red curves in (a) and (b) are logarithmic fits of Eqs. (5.1) and (5.8), respectively.

Bibliography

[1] R. G. Miller, S. Narayanaswamy, J. L. Tallon, and S. Brooker, New J. Chem. **38**, 1932 (2014).

[2] R. Kulamczewski, J. Olguin, J. A. Kitchen, H. L. C. Feltham, G. N. L. Jameson, J. L. Tallon, and S. Brooker, J. Am. Chem. Soc. **136**, 878 (2014).

[3] M. Shigeno, Y. Kushida, and M. Tamaguchi, Chem. Commun. **52**, 4955 (2016).

[4] S. Singh, M. R. Fitzsimmons, T. Lookman, J. D. Thompson, H. Jeen, A. Biswas, M. A. Roldan, and M. Varela, Phys. Rev. Lett. **108**, 077207 (2012).

[5] R. Xie, C. T. Bui, B. Varghese, Q. Zhang, C. H. Sow, B. Li, and T. L. Thong, Adv. Funct. Mater. **21**, 1602 (2011).

[6] Ö. Can and N. B. Holland, Biochemistry **52**, 8745 (2013).

[7] C. P. Garnham, R. L. Cambell, and P. L. Davies, PNAS **108**, 7363 (2011).

[8] F. Zhong, J. X. Zhang, and G. G. Siu, J. Phys.: Condens. Matter **6**, 7785 (1994); F. Zhang, and J. X. Zhang, Phys. Rev. **E** 51, 2898 (1995); F. Zhang,

J. X. Zhang, and X. Liu, Phys. Rev. E **52**, 1399 (1995); F. Zhong, and J. X. Zhang, Phys. Rev. Lett. **75**, 2027 (1995).

[9] J. X. Zhang, F. Zhong, and G. G. Siu, Solid State Commun. **97**, 847 (1996).

[10] M. S. Heo, Y.H. Kim, K. Kim, G. Moon, J. Lee, H.R. Noh, M. I. Dykman, and W. Jhe, Phys. Rev. E. **82**, 031134 (2010).

[11] S. Yildz, O. Pekcan, A. N. Berker, and H. Ozbek, Phys. Rev. E. **69**, 031705 (2004).

[12] K. A. Takeuchi, Phys. Rev. E **77**, 030103(R) (2008).

[13] Y-Z. Wang, Y. Li, and J-X. Zhang, J. Chem. Phys. **134**, 114510 (2011).

Chapter 6

Other Works in the ^{87}Rb MOT System

6.1 The Evaporative Cooling of ^{87}Rb Atoms in a Magnetic Trap

In order to obtain the Bose-Einstein Condensate (BEC) of ^{87}Rb, we used a double-MOT system to overcome a contradiction about the vacuum in the second chamber as shown in Fig. 6.1. The experimental setup in detail was described in our previous works [1]. The pressure of the 2nd chamber is below 10^{-11} Torr. First, we trapped the Rb atoms in the 1st chamber which is called 1st MOT and transferred to the 2nd chamber by the pushing beam which is a resonant beam of Rb atom. The pushing beam is focused 3 mm above and 1 cm in front of the 2nd MOT's center to avoid scattering with the trapped atoms

in 2nd chamber. After transferring, all processes for making the BEC proceeds in the second chamber so, the second chamber is called science chamber. For achieving BEC, the system is needed to have below the critical temperature. But laser cooling method has the fundamental limit since the kicking by photons. Then the cold atoms in MOT are transferred to the magnetic trap without the lasers. The atoms were trapped in the $|F, m_F\rangle = |1, -1\rangle$. The magnetic quadrupole trap was calculated as shown in Fig. 6.2. The Hamiltonian of atoms in a magnetic quadrupole trap can be expressed as [4]

$$H(\mathbf{r}) = -\boldsymbol{\mu} \cdot \boldsymbol{B}(\boldsymbol{r}), \tag{6.1}$$

where $\boldsymbol{\mu}$ is the total magnetic moment of the atoms, the magnetic field of the system is $\boldsymbol{B}(\boldsymbol{r}) = B'(x, y, -2z)$. And we assume the atoms move slowly in this magnetic field, then the potential of magnetic trap for the $F = 1$ manifold is written by

$$E_{m_F} = U_{m_F} = g_F m_F \mu_B |\boldsymbol{B}(\boldsymbol{r})| \tag{6.2}$$

$$= g_F m_F \mu_B B' r \tag{6.3}$$

where μ_B is the Bohr magneton, m_F is the projection of the total angular momentum of the atom on the magnetic field axis, B' is the magnetic field gradient, and $r = \sqrt{x^2 + y^2 + (2z)^2}$.

After the loading in the magnetic trap, we apply a radio frequency (RF) field, which is the transition frequency from the magnetic sub-level of the ground

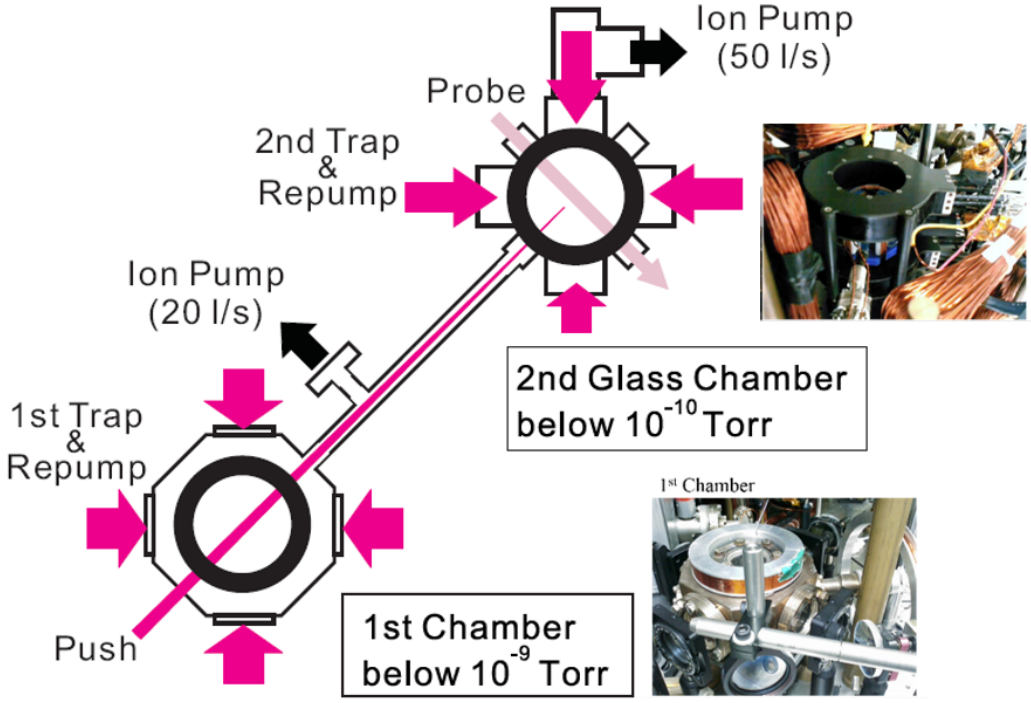

Figure 6.1: Schematic diagram of the double MOT system.

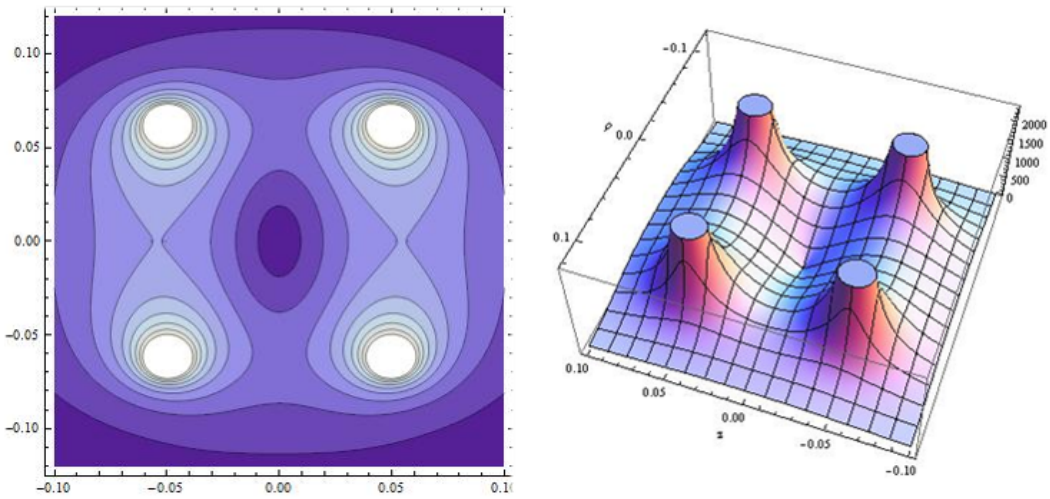

Figure 6.2: The calculation of the magnetic quadrupole trap.

state ($F = 1$) of ^{87}Rb atom, $m_F = -1$ to $m_F = +1$. We use a small, few turns of loop antenna which is attached 2nd chamber to transmit the RF-field to the trapped atoms. The excited atoms by RF field feel the magnetic potential contrary, then the excited atoms which relatively have large momentum escape the trap. We succeeded the evaporative cooling in the magnetic trap as shown in Fig. 6.3. The absorption imaging method which was used in Fig 6.3 was described in detail in our previous works [1]. The density of atomic cloud increased after evaporative cooling although the number of atoms decreased as shown in In Fig. 6.3. Since the hotter atoms were kicked out by RF field.

6.2 The Time-averaged Orbiting Potential (TOP) Trap

At the center of the magnetic trap, the magnetic field is zero. Thus the spin of atoms can be reversed at the center of the trap, this is called the Majorana spin-flip transitions [2]. The spin-fliped atoms escape the trap because they feels the trap reversely and they become the trap loss. When the atoms get colder , the trap loss is dominant since the colder atoms are in the center of the trap. As shown in Fig. 6.4, the evaporatively cooled atoms in the magnetic trap got colder but the density of atoms does not increase. Therefore, the system needs a way to remove the magnetic field is zero. We used two methods for eliminating the trap loss, time-averaged Orbiting Potential (TOP) trap and hybrid trap (the conventional magnetic qudrupole trap with the dipole trap)

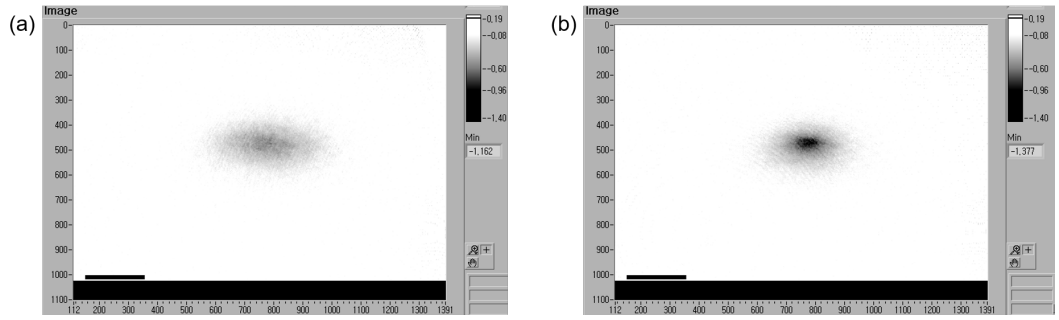

Figure 6.3: The absorption images of the atomic clouds, (a) before the evaporative cooling (b) after the evaporative cooling. The density of atomic clouds increased.

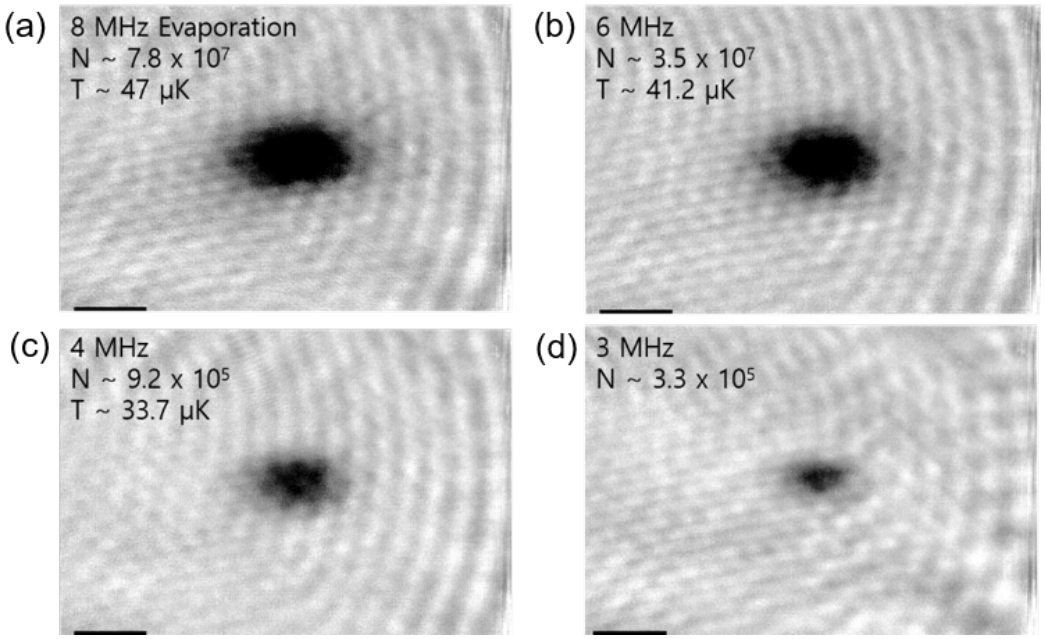

Figure 6.4: Typical images of the atomic clouds after evporative cooling. From (a) to (d) were applied different frequencies of the RF field.

The time-averaged Orbiting Potential (TOP) trap was realized by an ordinary magnetic quadrupole trap with the additional magnetic field which varies periodically [3]. And TOP trap is consist of the anti-Helmholtz coil pair and the two coil pair which is generated the spatially uniform and rotating bias field on x,y-axis which is perpendicular to the anti-Helmholtz axis as shown in Fig. 6.5. The bias field was applied by a function generator and had a $7kHz$ sine signal. The bias frequency ($7kHz$) is faster than the atomic motion ($\sim$a few $100Hz$) and is slower than transition frequency (order of MHz). Therefore, the bias field does not affect the trapped atoms The magnetic field of the TOP trap is

$$\boldsymbol{B}(\boldsymbol{r}) = (B'x + B_0 cos\omega t, B'y + B_0 sin\omega t, -2B'z), \tag{6.4}$$

the bias field is

$$\boldsymbol{B_t}(\boldsymbol{r}) = (B_0 cos\omega t, B_0 sin\omega t, 0). \tag{6.5}$$

And the magnetic potential of the TOP trap is written by

$$U_{TOP} \cong g_F m_F \mu_B B_0 + \frac{g_F m_F \mu_B B'^2}{4B_0} \left[x^2 + y^2 + 8z^2\right]. \tag{6.6}$$

The potential of TOP trap, the equation (6.6), has the nonzero value at the center of the trap ($r = 0$). It prevented that the atoms escape the trap at center. By forced the RF-field, we tried to evaporative cooling in the TOP trap. After the evaporation in the TOP trap, the density of atomic cloud decreased only as shown in Fig. 6.6. These results say that the colder atoms were blown up also by the fluctuations which were due to unknown reasons.

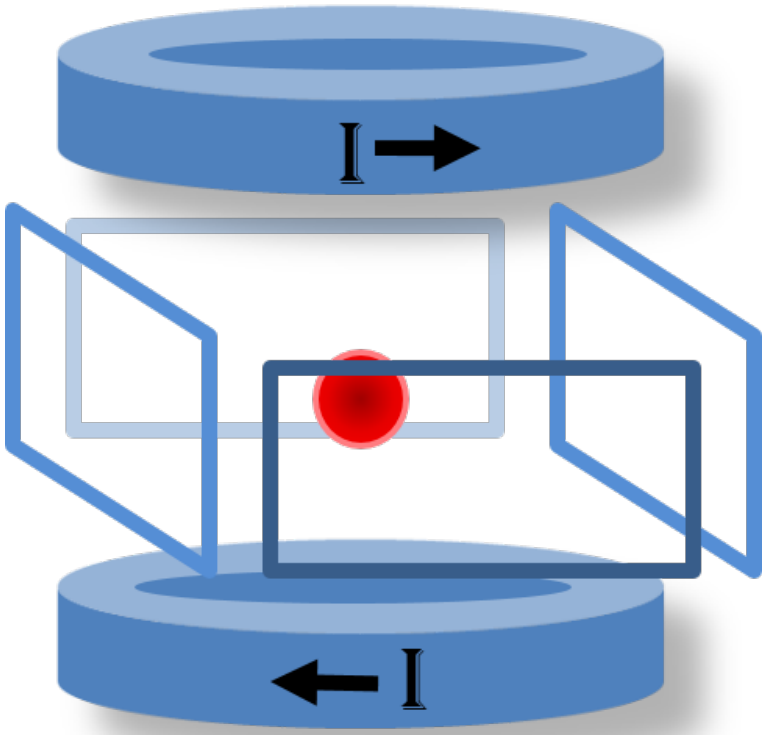

Figure 6.5: Schematic diagram of the time-averaged Orbiting Potential (TOP) trap.

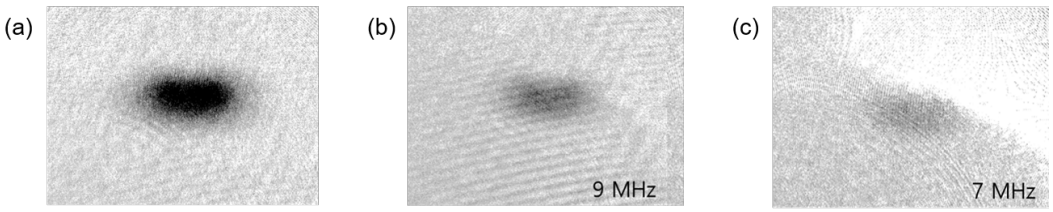

Figure 6.6: The absorption images of trapped atoms (a) in TOP trap without evaporative cooling, (b) and (C) are the images after evaporation.

6.3 The Hybrid Trap

The neutral atoms are interacted with far from the resonant beam, as a result, the atoms are trapped the optical dipole trap. The hybrid trap is one of the ways to achieve BEC. It is consisted of the magnetic quadrupole trap and the dipole trap [5,6]. The dipole beam blocks the hole near the center of the magnetic trap. The optical dipole force comes from the dispersive interaction of the induced dipole moment of neutral atoms with the intensity gradient of the light field [7]. When the electric field of the far-detuned dipole laser induces a dipole moment $\boldsymbol{p} = \alpha \boldsymbol{E}$, where α is the complex polarizability and $\mathbf{E}$ is the electric field of the laser. The dipole potential is given by

$$U_{dip} = -\tfrac{1}{2}\langle \boldsymbol{p} \cdot \boldsymbol{E} \rangle \tag{6.7}$$

$$= \tfrac{1}{2\epsilon_0 c} Re(\alpha) I, \tag{6.8}$$

where $I = 2\epsilon_0 c |\boldsymbol{E}|^2$ is the field intensity. With rotating-wave approximation, the dipole potential simplifies to

$$U_{dip} = \frac{3\pi c^2}{2{\omega_0}^2} \frac{\Gamma}{\Delta} I(\boldsymbol{r}), \tag{6.9}$$

where ω_0 is the resonant frequency of the atom, Γ is the on-resonance damping rate which is corresponded to the spontaneous decay rate of the excited level, and Δ is the detuning. The process of induction of the dipole trap in detail was descibed in [7].

We use 850 nm and 150 mW diode laser for dipole trap and, it was aligned along the center of the magnetic trap as shown in Fig. 6.8. A schematic

diagram of the hybrid trap is shown in Fig. 6.7. The intensity of dipole laser is controlled by an AOM and the laser passes through an optical fiber for a gaussian profile. The optical fiber and the focusing lens of dipole laser are attached on an XYZ-translator to control finely the position. In our experiment, the beam waist of the dipole laser is 18 μm and the power in the trap is 15 mW, then the calculated trap depth is 13 μK. The trapped atoms were cooled below few μK after evaporation, so the depth of dipole trap was enough. But we could not achieve BEC with the hybrid trap. We consider that the dominant reasons for this failure are the deviated align of the point of view and center of the trap, this mismatch was about a few mm order as shown in Fig. 6.9 (b) and it affected significantly to the trapped atom with compared to the size of an atomic cloud ($\cong 1mm$). Another reason is that the windows of glass cell in 2nd chamber acted a lens as shown in Fig. 6.9 (a). We changed the glass cell [Fig. 6.9 (c)] and built up again as shown in Fig. 6.9(d) and (e). We obtain 1st MOT and 2nd MOT in new setup as shown in Fig. 6.10 but could not progress to next step because of vacuum problems.

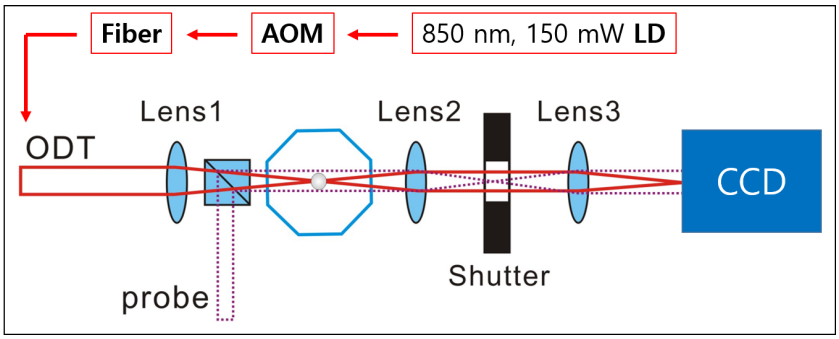

Figure 6.7: The shematic diagram of the hybrid trap.

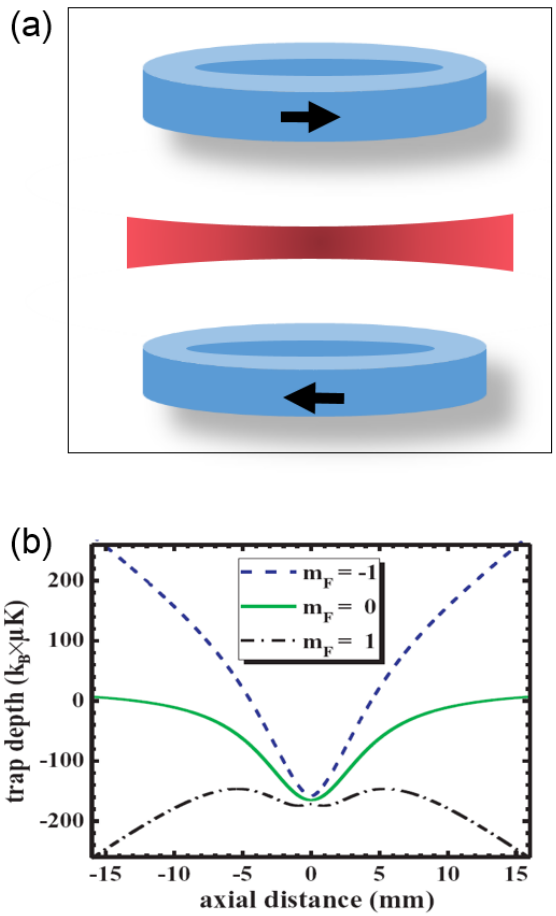

Figure 6.8: (a) The hybirid trap is consisted of the anti-Helmholtz coil and a optical dipole beam (b) A potential diagram of the hybrid trap [8].

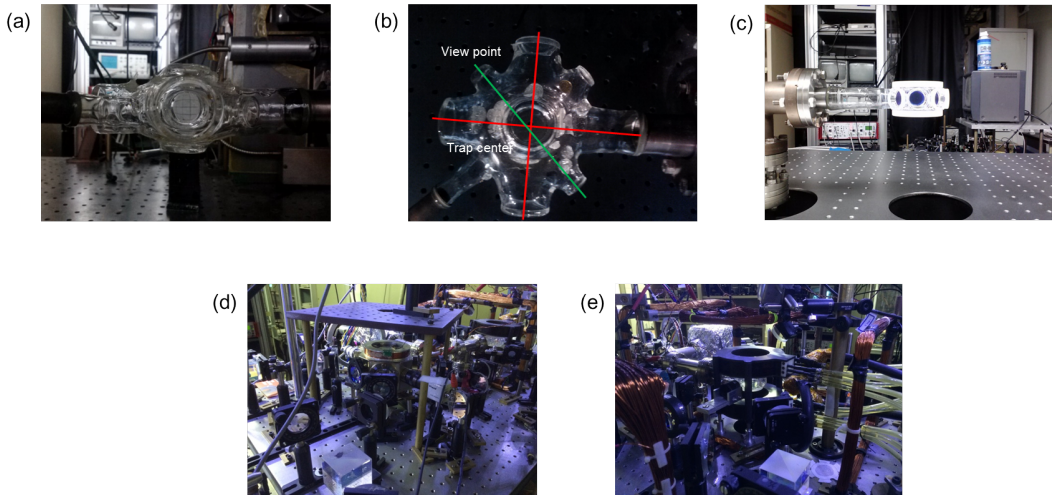

Figure 6.9: The pictures of the glass cell at (a) a side view, (b) a top view, and (c) is new glass cell. The pictures of the experimetal setup of (d) 1st MOT system and (e) 2nd MOT system.

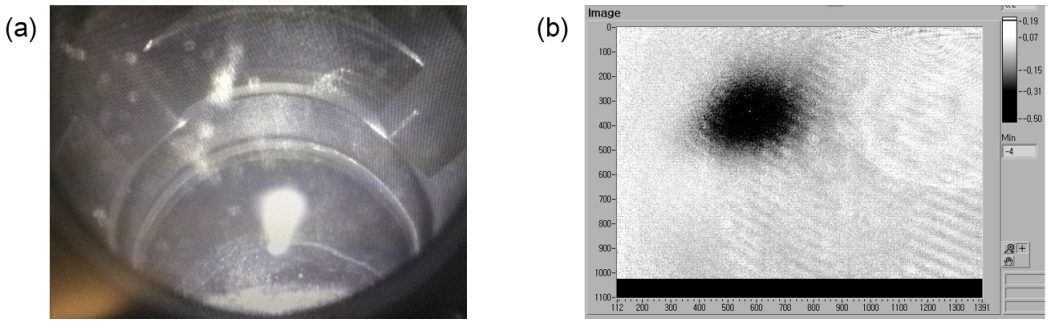

Figure 6.10: (a) A picture of the 1st MOT and (b) an absorption image of 2nd MOT.

6.4 A Oscillatory Motion in the Magnetic Quadrupole Trap

The atoms in a magneto-optical trap undergo overdamped simple harmonic motion in typical conditions by the trapping laser [8]. It requires high trapped atoms density to achieve condensate, thus the larger magnetic field is applied for the high density of trapped atoms after MOT sequence , which is called compressed MOT (CMOT). We observed an oscillatory motion of atomic clouds in the magnetic trap. The oscillation occurred when the holding time of the atoms in cMOT was relatively short. In this section, we will investigate the cause of this phenomenon, and describe a physical quantity that can be obtained through this.

6.4.1 Experimental Methods

Our experimental setup is ^{87}Rb MOT system using two chambers. We recaptured the ^{87}Rb atoms in the 2nd chamber after the MOT was pushed from the 1st chamber by the pushing laser which has red detuned (2Γ) frequency from the resonance of trap line. The detailed experimental setup and experimental conditions are described in our previous works [1,9]. After magneto-optical trap in 2nd chamber, we applied the magnetic field more tightly. This process is called the compressed MOT (cMOT). The magnetic field gradient which is related to the additional momentum of the atoms increased more than twice from $25.9 G/cm$ to $64.11 G/cm$ by increasing the applied current to the anti-Helmholtz

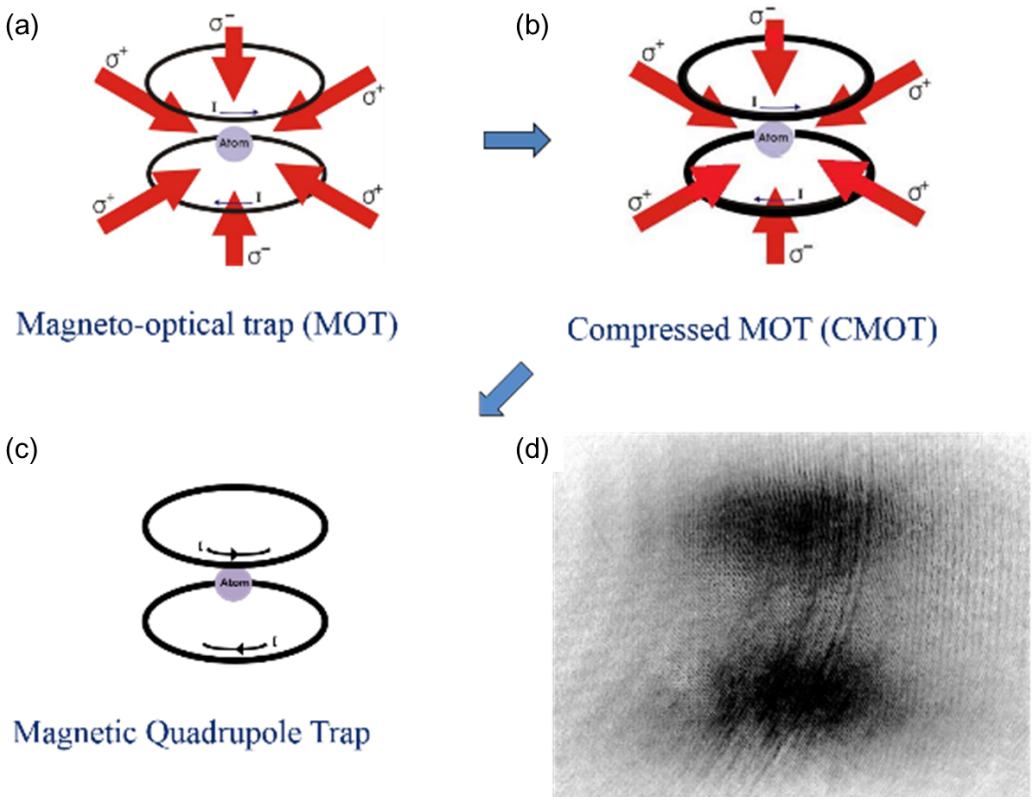

Figure 6.11: A schematic diagram of sequences from the MOT to the magnetic trap. (a) the MOT, (b) cMOT, (c) magnetic trap, and (d) an absorption image of two separated atomic clouds by oscillation.

coil from $40A$ to $100A$. In this sequence, if the holding time was shorter than $10ms$, and after that, the atoms were transferred the magnetic trap, we observed the oscillatory motion of the atomic clouds as shown in Fig. 6.11 (d).

6.4.2 Experimental Results and Discussion

To describe the motion of the atoms in a MOT, the total force on the atom is given by $F = F_+ + F_-$ in the low intensity limit for two-level atom. Where

$$F_\pm = \pm\frac{\hbar k\gamma}{2}\frac{s_0}{1 + s_0 + (2\delta_\pm/\gamma)^2} \tag{6.10}$$

respectively, where k is the wave, δ is the detuning, γ is the natural linewidth, and $s_0(= I/I_0)$ is the normalized laser intensity with I_s being the saturation intensity [10, 11]. When the Doppler and Zeeman shifts are small compared to the detuning, the force from Eqn. (6.10) becomes

$$F = -\beta v - \kappa r, \tag{6.11}$$

where κ is the spring constant which is given by

$$\kappa = \frac{g_F\mu_B B'}{\hbar k}\beta. \tag{6.12}$$

And the damping coefficient β is given by

$$\beta = \frac{8\hbar k^2}{m}\frac{s_0(\delta/\gamma)}{(1 + 4\delta/\gamma^2)^2}, \tag{6.13}$$

where μ_B is Bohr magneton and m is the mass of an atom [10]. The atoms in MOT have overdamped harmonic motion which is the force of Eqn. (6.11). The restoring time to the center of the trap is about several ms for typical conditions. When the holding time in cMOT was shorter than $10ms$, the atom could not loose their additional momentum which is from the increased magnetic field in the cMOT during the holding time. Therefore, the atoms which are transferred to the magnetic trap moved toward the opposite direction. The magnetic

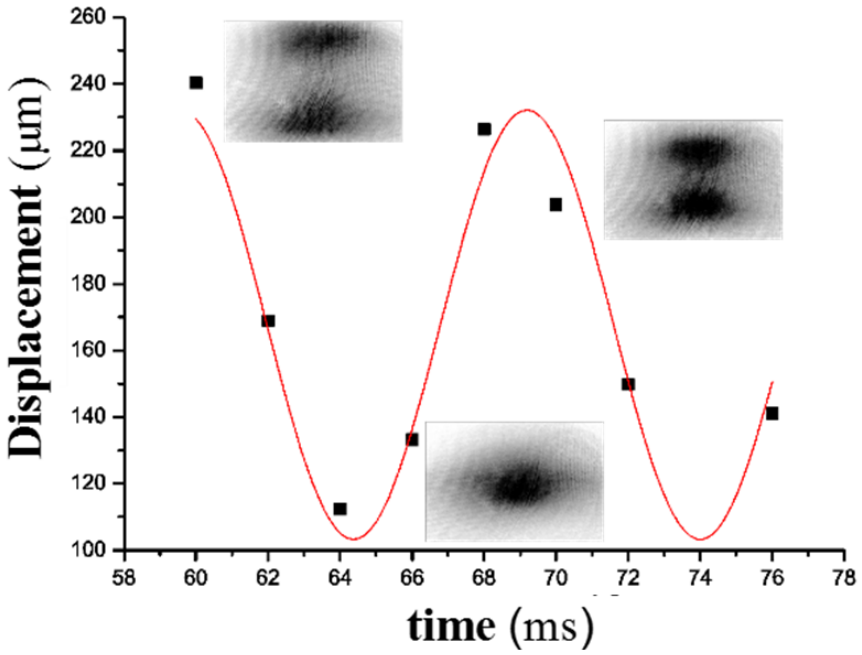

Figure 6.12: The displacement between the two separated atomic clouds verses the time with the absorption images at some points.

quadrupole trap is the conservative system, since there is no the damping of system, resonant frequency laser but trap loss in the center of the trap exist still. Therefore perturbated atoms by the compressed magnetic field move in the magnetic trap freely. We obtained the oscillatory motion of the atom in the magnetic trap as shown in Fig. 6.12. The holding time in cMOT (t_h) is $2ms$ and the magnetic field gradient B' is 164.46 G/cm.

To investigate the cause of the oscillation, we obtained absorption images of the atoms with changing the holding time from $2ms$ to $12ms$ in cMOT sequence and the staying time in the magnetic trap was same. In the Fig. 6.13,

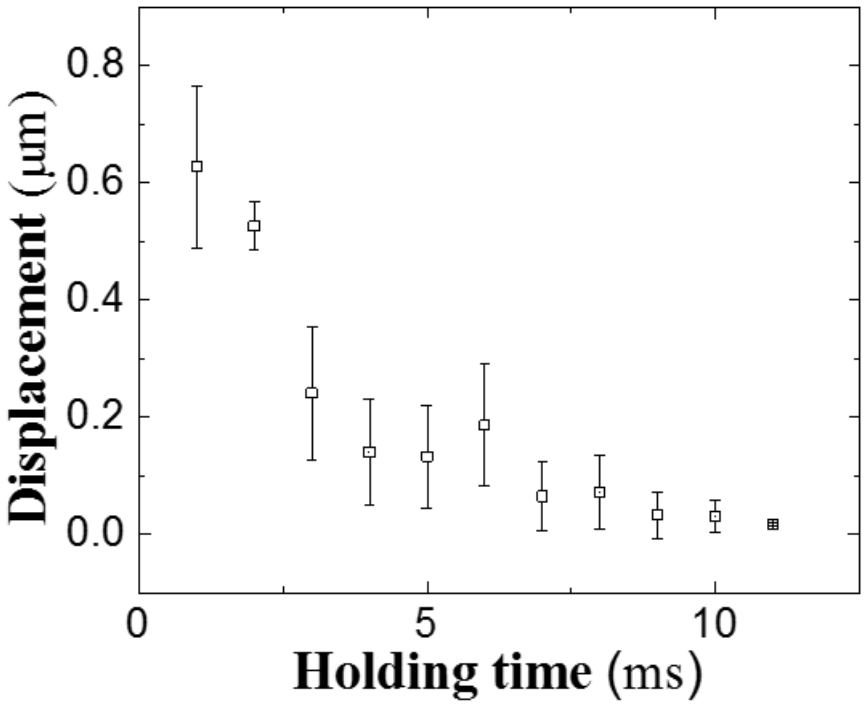

Figure 6.13: The maximum displacement of the two separated atomic clouds verses the holding time in cMOT.

the maximum displacement between the two atomic clouds decreased, when the holding time in the cMOT increased. The atoms which stayed in cMOT longer than $10ms$ had enough restoring time to the center of the trap. As results, we observed that the separation of atomic clouds did not emerge over 10ms of holding time in cMOT. As the result, we proved that the oscillatory motion of the trapped atoms in the magnetic trap occurs due to the short cMOT holding time less than $10ms$.

Bibliography

[1] D. Yum, J. Park, W. Lee, and W. Jhe, J. Kor. Phys. Soc. **60**, L1 (2012).

[2] I. Bloch, T. W. Hansch, and T. Esslinger, Nature. **403**, 166 (2000).

[3] D. M. Brink and C. V. Sukumar, Phys. Rev. A **74**, 035401 (2006).

[4] W. Petrich, M. H. Anderson, J. R. Ensher, and E. A. Cornell, Phys. Rev. Lett. **74**, 3352 (1995).

[5] Y.-J. Lin, A. R. Perry, R. L. Compton, I. B. Spielman, and J. V. Porto, Phys. Rev. A **79** 063631 (2009).

[6] M. Zaiser, J. Hartwig, D. Schlippert, U. Velte, N. Winter, V. Lebedev, W. Ertmer, and E. M. Rasel, Phys. Rev. A **83**, 035601 (2011).

[7] R. Grimm, M. Weidemüller and Y.B. Ovchinnikov, Advances in Atomic, Molecular and Optical Physics **42**, 95 (2000).

[8] C. J. Foot, *Atomic Physics* (Oxford, New York, 2005).

[9] D. Yum, Ph. D. thesis, Seoul National University, 2012.

[10] H. J. Metclf, P. van der Straten, *Laser Cooing and Trapping* (Springer, 1999).

[11] K. Kim, K-H. Lee, M. Heo, H-R. Noh, and W. Jhe, Phys. Rev. A **71**, 053406 (2005).

Chapter 7

Conclusions

The thermal hysteresis and critical slowing down are ubiquitous phenomena that characterize the behavior of the system and it has been studied in various fields, ranging from nonlinear dynamics in economics and finance to anti-freeze proteins in a biologic system. We have demonstrated the critical dynamics phenomena which are critical slowing down and hysteresis in parametrically modulated MOT system. The spontaneous symmetry breaking (SSB) transition is shown in the system when the total number of atoms increase and exceed the certain number which is called critical number. In our previous works, we analyzed the stationary state of the SSB transition and its critical behavior. But when the total number of atoms, an important factor of the SSB transition, changes constantly with time, a hysteresis occurs in the transition.

In order to investigate the hysteresis, we observe the critical slowing down in our system by measuring the relaxation time at each point. In addition,

we theoretically described the relaxation time and showed that the numerical results from the mean-field equation of motion are matched the experiments. To characterize the hysteresis, we had the theoretical approaches and the scaling of the hysteresis. As a result, the hysteresis has the scaling exponents as theoretical expectation and it can be analogous to thermal hysteresis in mean-field model.

In summary, we observed the thermal hysteretic scaling behavior in a modulated MOT system. We obtained the hysteresis loop by sweeping the total number of atoms with a uniform speed. The scaling exponent of the hysteresis loop area with sweeping was 0.64 ± 0.04, which was in excellent agreement with the expected value in the mean-field model. The scaling exponent of the hysteresis width was obtained to be 0.44 ± 0.025. We provided a new method for studying thermal hysteresis. Moreover, if the number decreasing (increasing) process was reversed before the system went to an equilibrium state, the hysteresis loop was not closed at the end of the decreasing (increasing) process. This suggests a glassy behavior, and thus a further study of the glass transition is in progress.

We succeeded to cool the trapped ^{87}Rb atoms until $30\mu K$ in the magnetic quadrupole trap by the evaporative cooling method with the RF(radio frequency) field. After then, for achieving Bose-Einstein condensate (BEC), we tried to the time-averaged orbiting potential (TOP) trap and hybrid trap which is consist of typical magnetic quadrupole trap and optical dipole trap. Even though we had been not cooled the trapped atom to the critical temperature of BEC, the experimental results of the trapping and cooling atoms in various trap

help our further step becomes closer the BEC. In addition, we observed oscillatory motion in magnetic quadrupole trap by the short compressed magneto-optical trap (cMOT) holding time. We investigated the cause of this oscillation by measuring maximum displacement with the cMOT holding time from $2ms$ to $12ms$ and we proof that the cause of the oscillatory motion of atoms is the not enough restoring time in the cMOT process.

Appendices

Appendix A

Numerical Calculation of the Mean-field Equation of Motion of Order Parameter

In this chapter, we present the numerical calculation of the mean-field equattion of motion as described in chapter 4 [1,2]. These results were calculated by Mathematica program code. And to determine the compatibility of the expansion of the mean-field equation, we calculated the expanded mean-field equattion of motion up to cubic term.

<The Equation of motion of Order parameter>

- Plot with Experimental data

```
Quit[]

Off[General::spell1];
Off[General::spell];


SetDirectory["C:\\Users\\Wanhee\\Dropbox\\연구\\critical slowing down\\20150502-0506 (theta,x)"]
```

```
C:\Users\Wanhee\Dropbox\연구\critical slowing down\20150502-0506 (theta,x)
```

```
Dexp = Import["t001.dat", "Table"];
Iexp = Import["t002.dat", "Table"];


τ = 1(*2W0=1/τ, W0 is the transition rate*);
λ0- = 1.8;
λ0+ = 0.1;
R- = 0.03433;
R+ = 0.04055;
finaltime = 60;
x0+ = 0.02;
θ- = (λ0- - 1) - R- * t;
θ+ = (λ0+ - 1) + R+ * t;
```

< Cosh, Sinh model >

```
(* Numerical calculation *)
sol3 = NDSolve[{τ x-'[t] == -x-[t] * Cosh[(θ- + 1) * x-[t]] + Sinh[(θ- + 1) * x-[t]],
    x-[0] == FindRoot[Tanh[λ0- * y] == y, {y, 1}][[1, 2]]}, x-, {t, 0, finaltime}];
f3 = Evaluate[x-[t] /. Flatten[sol3]];
sol4 = NDSolve[{τ x+'[t] == - x+[t] * Cosh[(θ+ + 1) * x+[t]] + Sinh[(θ+ + 1) * x+[t]], x+[0] == x0+},
   x+, {t, 0, finaltime}];
f4 = Evaluate[x+[t] /. sol4];
Decrease1 = ParametricPlot[{θ-, f3}, {t, 0, finaltime}, PlotRange → All,
   PlotStyle → {Green, Thick}];
Increase1 = ParametricPlot[{θ+ - 0.55, f4}, {t, 0, finaltime}, PlotRange → All,
   PlotStyle → {Green, , Thick}];
(* Experimental Data *)
DecExp = ListPlot[Dexp, PlotRange → All, PlotStyle → Black];
IncExp = ListPlot[Iexp, PlotRange → All, PlotStyle → Black];
Steady = Plot[x /. FindRoot[x == Tanh[(θ + 1) * x], {x, 0.5}], {θ, -0.5, 1}, PlotStyle → Red];
Show[DecExp, IncExp, Steady, Decrease1, Increase1, AxesLabel → {θ[t], x[θ, t]},
 PlotRange → {0, 1.2}]
```

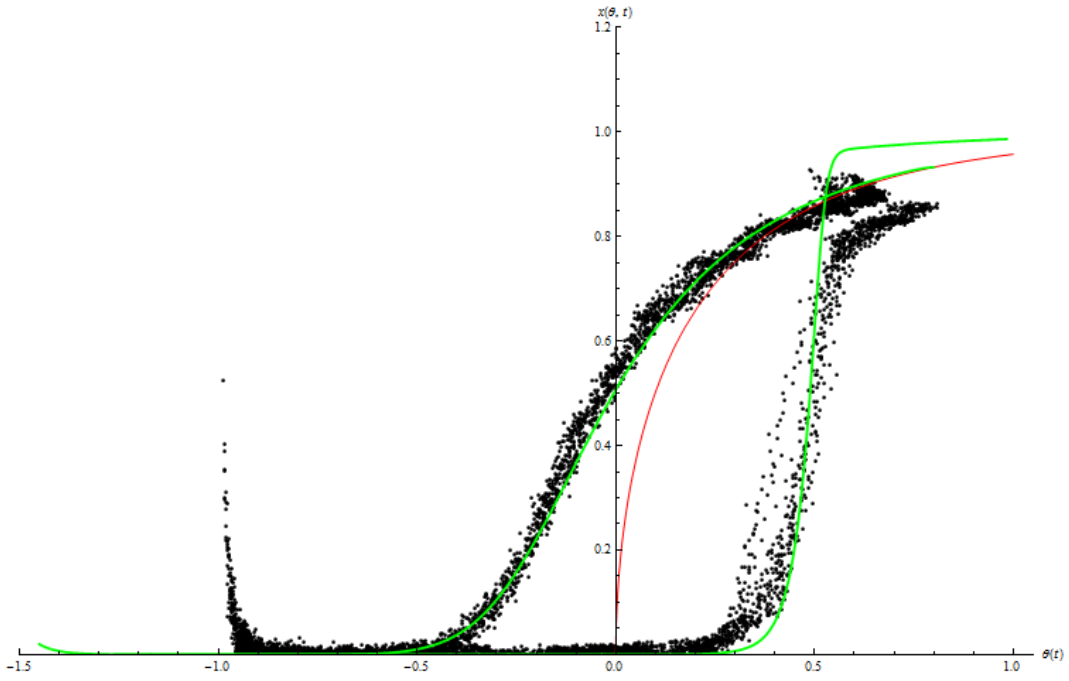
x(ϑ, t)
1.2
1.0
0.8
0.6
0.4
0.2
−1.5
−1.0
−0.5
0.0
0.5
1.0
ϑ(t)

```
(* Expand the eq O(x^3,t^3) *)
DeExp =
  NDSolve[
   {τ x⁻'[t] == ((-1 + (λ0)⁻) - R⁻ t) x⁻[t] +
       ((-1/2 ((λ0)⁻)^2 + 1/6 ((λ0)⁻)^3) + (R⁻ (λ0)⁻ - 1/2 R⁻ ((λ0)⁻)^2) t + (-R⁻²/2 + 1/2 R⁻² (λ0)⁻) t² - R⁻³ t³/6)
        x⁻[t]^3, x⁻[0] == FindRoot[Tanh[λ0⁻ * y] == y, {y, 1}][[1, 2]]}, x⁻, {t, 0, finaltime}];
InExp =
  NDSolve[
   {τ x⁺'[t] == ((-1 + (λ0)⁺) + R⁺ t) x⁺[t] +
       ((-1/2 ((λ0)⁺)^2 + 1/6 ((λ0)⁺)^3) + (-R⁺ (λ0)⁺ + 1/2 R⁺ ((λ0)⁺)^2) t + (-R⁺²/2 + 1/2 R⁺² (λ0)⁺) t² + R⁺³ t³/6)
        (x⁺[t])^3, x⁺[0] == x0⁺}, x⁺, {t, 0, finaltime}];
DeEx = Evaluate[x⁻[t] /. DeExp];
InEx = Evaluate[x⁺[t] /. InExp];
DeExpPlot = ParametricPlot[{θ⁻, DeEx}, {t, 0, finaltime}, PlotRange → All,
   PlotStyle → {Blue, Thick}];
InExpPlot = ParametricPlot[{θ⁺ - 0.55, InEx}, {t, 0, finaltime}, PlotRange → All,
   PlotStyle → {Blue, Thick}];
(* Expand the eq O(x^3) *)
DeExpX = NDSolve[{τ x⁻'[t] == θ⁻ x⁻[t] + 1/6 (-2 - 3 θ⁻ + (θ⁻)^3) x⁻[t]^3,
    x⁻[0] == FindRoot[Tanh[λ0⁻ * y] == y, {y, 1}][[1, 2]]}, x⁻, {t, 0, finaltime}];
InExpX = NDSolve[{τ x⁺'[t] == θ⁺ x⁺[t] + 1/6 (-2 - 3 θ⁺ + (θ⁺)^3) x⁺[t]^3, x⁺[0] == x0⁺}, x⁺,
   {t, 0, finaltime}];
DeExX = Evaluate[x⁻[t] /. DeExpX];
InExX = Evaluate[x⁺[t] /. InExpX];
XDeExpPlot = ParametricPlot[{θ⁻, DeExX}, {t, 0, finaltime}, PlotRange → All,
   PlotStyle → {Orange}];
XInExpPlot = ParametricPlot[{θ⁺ - 0.55, InExX}, {t, 0, finaltime}, PlotRange → All,
  PlotStyle → {Orange}]; Show[DecExp, IncExp, Steady, Decrease1, Increase1, DeExpPlot,
 InExpPlot, XDeExpPlot, XInExpPlot, AxesLabel → {θ[t], x[θ, t]}, PlotRange → {0, 1.2}]
```

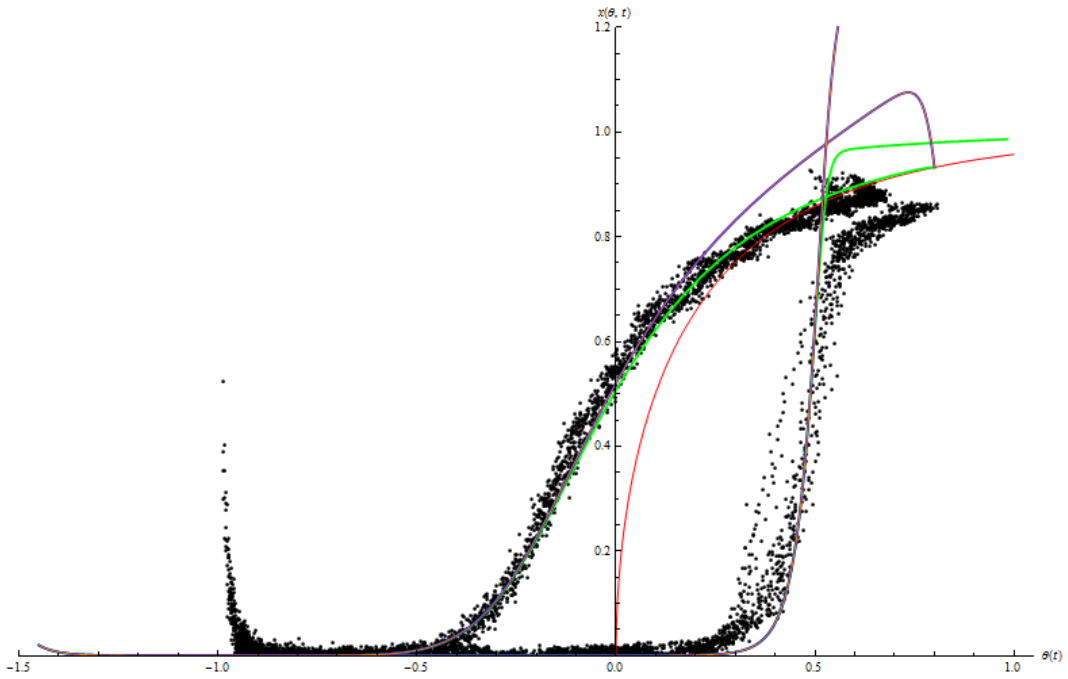
x(θ, t)
1.2
1.0
0.8
0.6
0.4
0.2
−1.5
−1.0
−0.5
0.0
0.5
1.0
θ(t)

Appendix B

Calculation of Hysteresis Loop Area

In order to obtain an area of the hysteresis loop which is presented in chapter 5, we used the mensuration by parts methods. First, we sorted the experimetal data to avoid a complexity of calculating as shown in Fig. B.1. Difference between original data and sorted data can be ignorable. The hysteresis loop area can be calculated as following equation :

$$\sum_j (\theta^d_{j+1} - \theta^d_j) \times x_j - \sum_k (\theta^i_{k+1} - \theta^i_k) \times x_k. \tag{B.1}$$

After then, we obtain the loop area by subtracting a calculated area of decreasing sequence form the one of increasing sequence as shown in Fig. B.2. For the calculation of the hysteresis loop area, we used the Lab-view programig language as shown in Fig. B.3. After loading two files as increasing and decreasing, The area was calculated by running the program. The data of calculted area can be

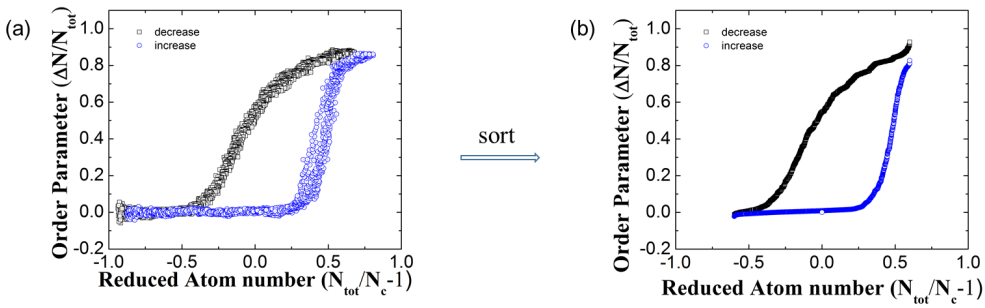

Figure B.1: Experimental data of the hysteresis by number sweeping. (a) is an original data and (b) is an sorted data.

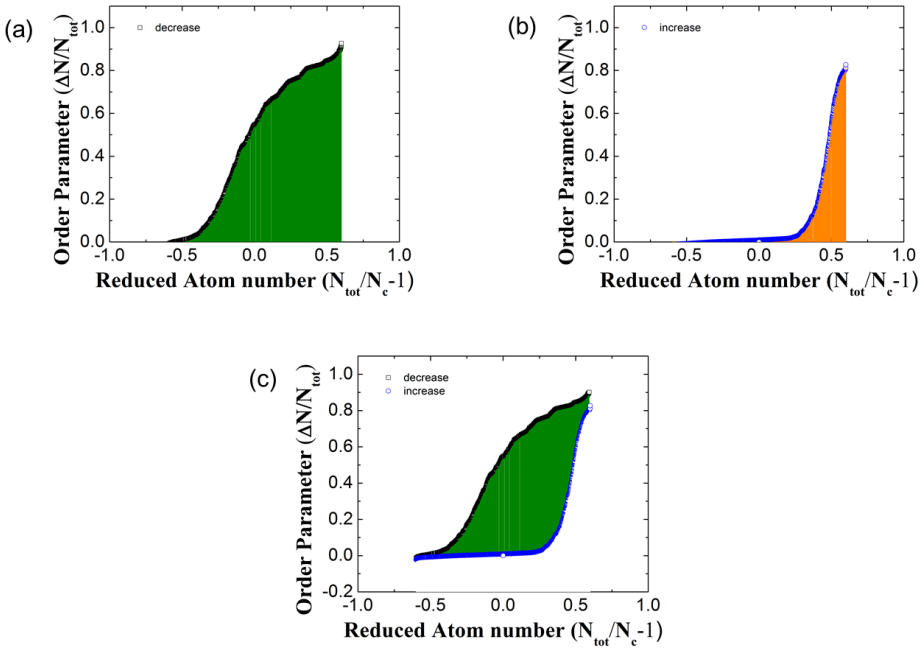

Figure B.2: The calculted area of (a) increasing, (b) decreasing and (c) subtracting.

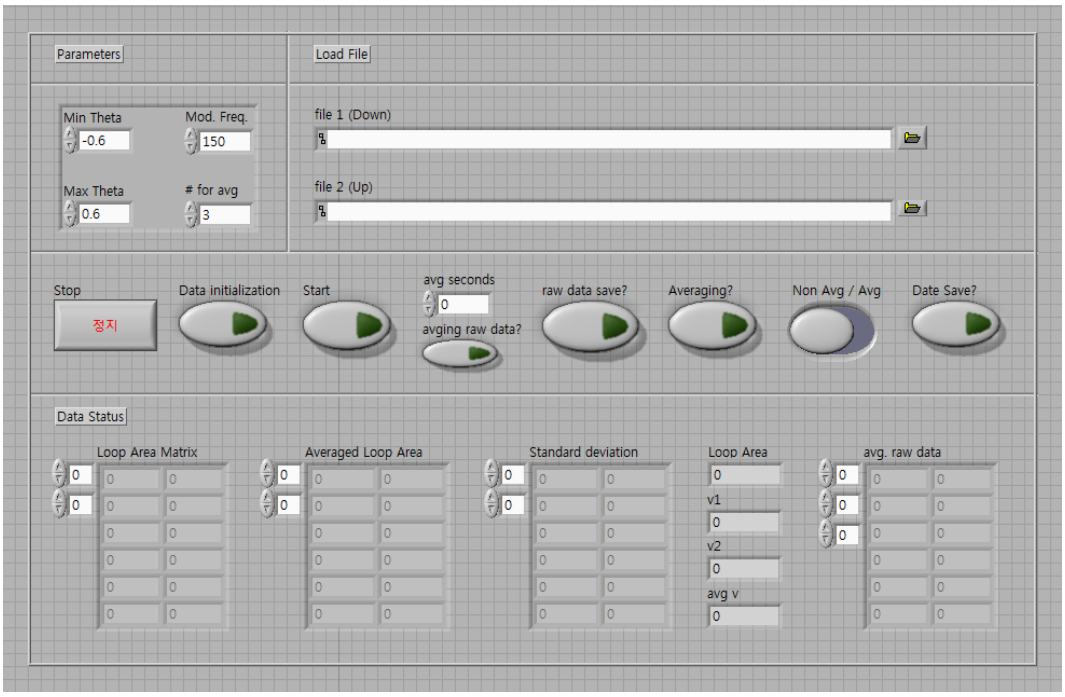

Figure B.3: Control panel for calculation of the hysteresis loop area

save as a law data or averaged data of same conditions.

Appendix C

Oscillatory Number Sweeping of Atoms

When the number increasing and decreasing of atoms are repeated periodically, the reduced total number of atoms $R(t)$ has triangular wave function over time as following equation [3]

$$R(t) = \frac{R_0}{2} + \frac{4R_0}{\pi^2} \sum_n \frac{1}{(2n-1)^2} cos[\frac{2(2n-2)\pi t}{T}]. \quad \text{(C.1)}$$

where R_0 is the maximum value of reduced total number of atoms and T is the period of the function. This function acts like a bias field effectively as shown in Fig. C.1. It is smililar to the bias field in other work [1]. The repeated number sweeping is worked by Labview program as shown in Fig. C.2. We choose to repeat or not the number sweeping in the part (a) of Fig. C.2 and other experimental condition in the part (b) of Fig. C.2. We expect to realize the glass transition system in our setup by the periodically repeated number

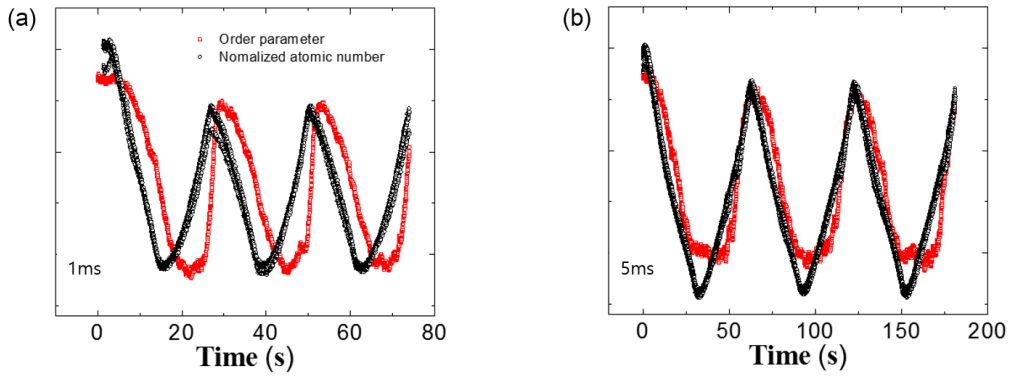

Figure C.1: A graph of the reponse of the order parameter with periodically repeated number sweeping. The sweeping rates are (a) 4.74×10^6 s^{-1} and (b) 1.87×10^6 s^{-1} .

sweeping. If the number increasing (decreasing) process is reversed before the system goes to equilibrium, the hysteresis loops is not closed at end of the process [4]. And this suggests the glssy behavior in our system, respectively.

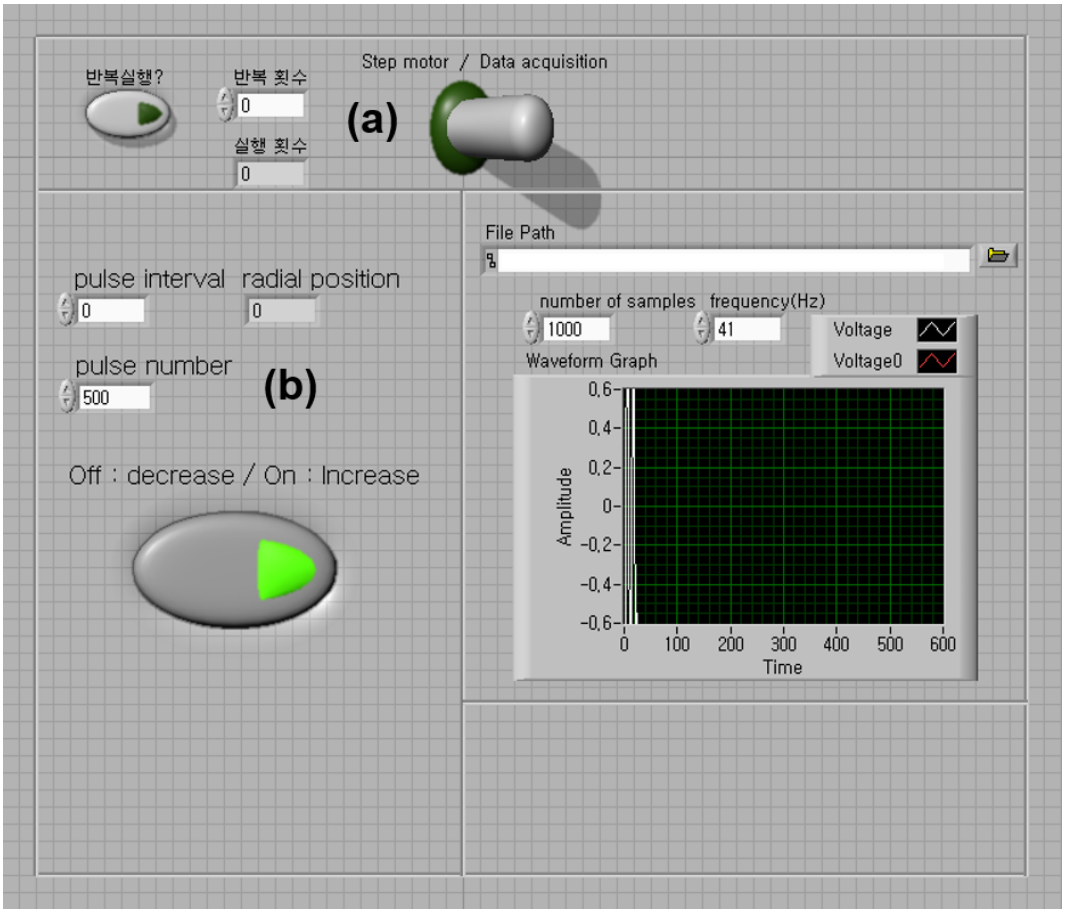

Figure C.2: Control panel for repeated number sweeping.

Bibliography

[1] Y. Kim, Ph. D. thesis, Seoul National University, 2011.

[2] M. Acharyya and B. K. Chakrabarti, Phys. Rev. B **52**, 6550 166 (1995).

[3] T. Myint-U, L. Debnath, *Linear Partial Differential Equations for Scientists and Engineers*, (Birkhäuser, Fourth Edition)

[4] S. Yildz, O. Pekcan, A. N. Berker, and H. Ozbek, Phys. Rev. E. **69**, 031705 (2004).

초 록

우리는 비선형적 조화진동자의 특성을 가지는 매개변수 변조된 광자기 덫에 포획된 루비듐 85 원자를 이용하여 동역학적 비평형 연구들을 수행하였다. 우리 시스템에서의 동역학적 쌍안정 상태는 광자기 덫에 사용되는 포획 레이저의 세기를 포획 고유 진동수의 두 배로 주기적 변조하여 얻어진다. 변조된 포획레이저 세기의 위상을 조절하여 매개변수 공진계와 더핑 진동자와 같은 비선형 동역학계를 구현하였고, 이를 통해 다양한 비선형 현상에 대한 연구가 수행되어 왔다.

시스템의 전체 원자 수가 특정한 원자 수 즉, 임계 수를 넘어서면 동역학적 쌍안정 상태에서 자발적 이산 시간병진 대칭성 깨짐 전이 현상(spontaneous discrete time-translational symmetry breaking transition)이 발생한다. 이 현상은 평균장 형태의 상전이 현상과 매우 유사한 양상을 보여준다. 특별히 원자 수를 일정한 속도로 바꿔줄 때 대칭성 깨짐 전이 현상에서 이력현상이 관측된다. 우리는 이력현상이 임계점 근처에서의 속도 둔화(slowing down)에 의해 발생됨을 예측하였다. 또한 이 이력현상이 어떠한 종류의 보편성(universality)을 가지는지 평균장 이론을 통하여 이론적 접근을 하였다. 이를 통해 우리는 원자 수 변화로 인한 이력현상이 평균장 형태의 열 이력현상과 유사함을 예측하였다.

우리는 전체 원자 수 변화에 따른 자발적 이산 시간병진 대칭성 깨짐 전이 현상에서 임의의 점에서의 풀림 시간(relaxation time)을 측정하였다. 이 실험결과들은 우리시스템에서 임계점에 접근할 때 풀림 시간이 증가하는 임계 속도 둔화 현상이 나타남을 입증하였다. 또한 각 지점에서의 풀림 시간을 질서매개변

수(order parameter)의 평균장 운동방정식으로부터 이론적으로 기술하였다. 이 이력현상의 물리적 특성을 살펴보기 위해 이력곡선의 면적과 이력넓이에 대한 축적지수(scaling exponent)를 실험적으로 측정하였다. 이 측정결과는 우리 시스템에서 나타난 이력현상이 평균장 형태를 따르는 다른 시스템에서의 열 이력과 유사함을 증명하였다. 주기적으로 변조된 저온 원자 시스템에서의 열적 이력 현상의 연구 결과를 바탕으로 우리 시스템은 분자 스위칭, 열에 의한 금속-절연체 전이(MIT), 부동단백질(AFPs) 등에서 연구되고 있는 열 이력현상 이해를 위한 좋은 모형이 될 것으로 기대한다.

주요어 : 비평형, 매개변수 공진, 이산 시간병진 대칭성 깨짐, 평균장 이론, 열적 이력현상, 임계 속도 둔화, 규격 행동

학 번 : 2009-20422